### Title

An Excitatory Circuit in the Perioculomotor Midbrain for Non-REM Sleep Control




### Journal

Cell, 177(5)

### ISSN

0092-8674



### Authors

Zhang, Zhe
Zhong, Peng
Hu, Fei
et al.



### Publication Date

2019-05-01

### DOI

10.1016/j.cell.2019.03.041

Peer reviewed

Article

Cell

# An Excitatory Circuit in the Perioculomotor Midbrain for Non-REM Sleep Control

## Graphical Abstract

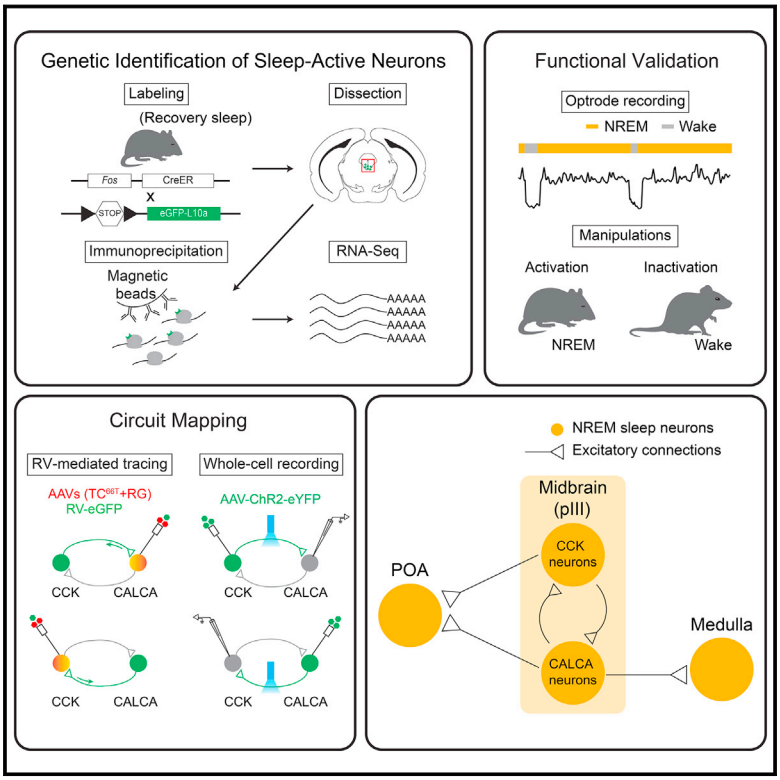


## Highlights

- Activity-dependent genetic labeling and gene profiling identify sleep-active neurons
- CALCA-expressing glutamatergic neurons in pIII are NREM active and NREM promoting
- pIII CCK neurons are NREM promoting and are reciprocally connected to CALCA neurons
- Both cell types send long-range excitatory projections to other sleep-promoting areas

## Authors

Zhe Zhang, Peng Zhong, Fei Hu, ..., Shinjae Chung, Richard D. Palmiter, Yang Dan

## Correspondence

ydan@berkeley.edu

## In Brief

Identification of sleep-active excitatory midbrain neurons that are interconnected and promote sleep via long range projections to other sleep centers of the mouse brain.

Zhang et al., 2019, Cell *177*, 1–15
May 16, 2019 
https://doi.org/10.1016/j.cell.2019.03.041

CellPress

Please cite this article in press as: Zhang et al., An Excitatory Circuit in the Perioculomotor Midbrain for Non-REM Sleep Control, Cell (2019), https://doi.org/10.1016/j.cell.2019.03.041

Article

Cell

# An Excitatory Circuit in the Perioculomotor Midbrain for Non-REM Sleep Control

Zhe Zhang,[1,4] Peng Zhong,[1,4] Fei Hu,[1] Zeke Barger,[1] Yulan Ren,[1] Xinlu Ding,[1] Shangzhong Li,[2] Franz Weber,[1,5] Shinjae Chung,[1,5] Richard D. Palmiter,[3] and Yang Dan[1,6,*]

[1]Division of Neurobiology, Department of Molecular and Cell Biology, Helen Wills Neuroscience Institute, Howard Hughes Medical Institute, University of California, Berkeley, Berkeley, CA 94720, USA

[2]Department of Bioengineering, University of California, San Diego, La Jolla, CA 92093, USA

[3]Howard Hughes Medical Institute and Departments of Biochemistry and Genome Sciences, University of Washington, Seattle, WA 98195, USA

[4]These authors contributed equally

[5]Present address: Department of Neuroscience, Perelman School of Medicine, University of Pennsylvania, Philadelphia, PA 19104, USA

[6]Lead Contact

*Correspondence: ydan@berkeley.edu

https://doi.org/10.1016/j.cell.2019.03.041

## SUMMARY

The perioculomotor (pIII) region of the midbrain was postulated as a sleep-regulating center in the 1890s but largely neglected in subsequent studies. Using activity-dependent labeling and gene expression profiling, we identified pIII neurons that promote non-rapid eye movement (NREM) sleep. Optrode recording showed that pIII glutamatergic neurons expressing calcitonin gene-related peptide alpha (CALCA) are NREM-sleep active; optogenetic and chemogenetic activation/inactivation showed that they strongly promote NREM sleep. Within the pIII region, CALCA neurons form reciprocal connections with another population of glutamatergic neurons that express the peptide cholecystokinin (CCK). Activation of CCK neurons also promoted NREM sleep. Both CALCA and CCK neurons project rostrally to the preoptic hypothalamus, whereas CALCA neurons also project caudally to the posterior ventromedial medulla. Activation of each projection increased NREM sleep. Together, these findings point to the pIII region as an excitatory sleep center where different subsets of glutamatergic neurons promote NREM sleep through both local reciprocal connections and long-range projections.

## INTRODUCTION

In the 1890s, Ludwig Mauthner proposed the existence of a "sleep center" near the oculomotor nucleus (III) in the midbrain, based on his observations of human patients with sleep disorders (Foley, 2018). Since then, the notion of a sleep center has inspired numerous studies to identify the brain regions important for sleep generation. However, the proposed role of the perioculomotor (pIII) region in sleep regulation has been largely forgotten.

Following the pioneering work of von Economo (1930) and Nauta (1946), most of the studies on sleep regulation have focused on the preoptic area (POA) of the hypothalamus. Lesions in the POA cause severe insomnia (Lu et al., 2000; McGinty and Sterman, 1968; Sallanon et al., 1989); sleep-active neurons have been observed in the POA using multiple techniques (Alam et al., 2014; Gong et al., 2004; Sherin et al., 1996; Szymusiak et al., 1998; Takahashi et al., 2009; Zhang et al., 2015), and recent studies have begun to reveal their genetic identities (Chung et al., 2017). In addition to the POA, sleep-promoting neurons have also been observed in other brain regions. For example, activation of gamma aminobutyric acid (GABA)ergic neurons in the parafacial zone (Anaclet et al., 2014), the ventrolateral periaqueductal gray (Weber et al., 2015; Weber et al., 2018), the ventral tegmental area (VTA) (Yang et al., 2018; Yu et al., 2019), or adenosine $A_{2A}$ receptor-expressing neurons in the striatum (Oishi et al., 2017; Yuan et al., 2017) specifically promotes non-rapid eye movement (NREM) sleep, whereas subgroups of GABAergic neurons in the lateral hypothalamus (Jego et al., 2013; Konadhode et al., 2013; Tsunematsu et al., 2014) and the *zona incerta* (Liu et al., 2017) promote both REM and NREM sleep. With the exception of nitrergic/glutamatergic neurons in the median and medial preoptic area that are excited by external warmth (Harding et al., 2018), the vast majority of sleep-promoting neuronal populations are GABAergic, and their sleep-promoting effects are likely mediated by the inhibition of wake-promoting populations. Because some sleep-promoting GABAergic neurons have been shown to be preferentially active during sleep (Anaclet et al., 2014; Hassani et al., 2009), an important question is whether there are excitatory sleep-active neurons that provide input to these GABAergic sleep neurons.

In this study, we performed global screening for sleep-active neurons in the mouse brain using a newly developed activity-dependent genetic labeling technique (Guenthner et al., 2013; Ye et al., 2016). We found that calcitonin gene-related peptide

Please cite this article in press as: Zhang et al., An Excitatory Circuit in the Perioculomotor Midbrain for Non-REM Sleep Control, Cell (2019), https://doi.org/10.1016/j.cell.2019.03.041



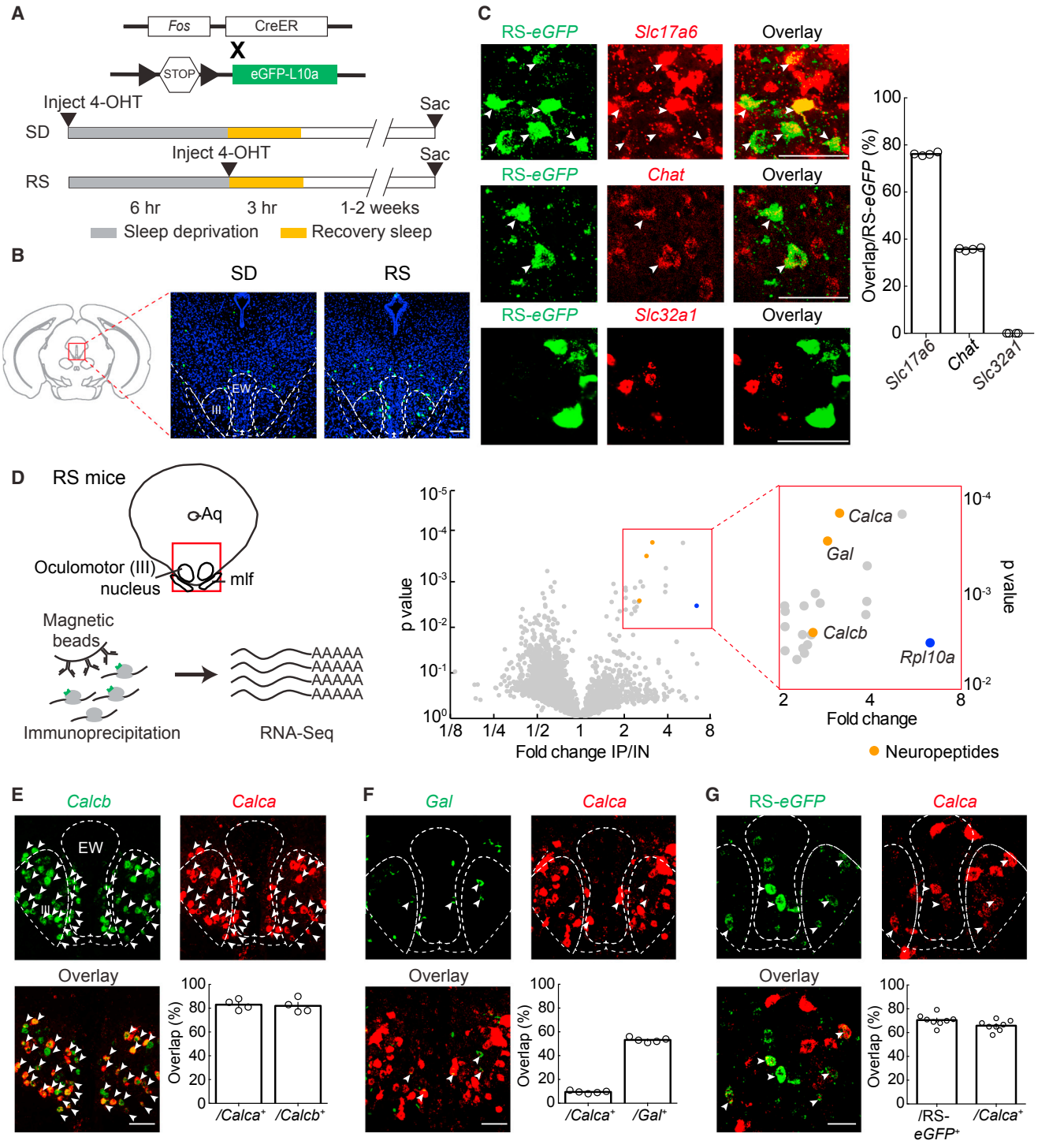


**Figure 1. Identification of Sleep-Active Neurons in the pIII Region**

(A) Experimental schematic. Mice expressing CreER under the *Fos* promoter are crossed with Cre-inducible reporter mice expressing EGFP-L10a. Each mouse undergoes 6 h of sleep deprivation (SD) and 3 h of recovery sleep (RS); 4-OHT was injected immediately before SD or RS to label wake- or sleep-active neurons, respectively.

(B) EGFP expression in the pIII region. Left: coronal diagram of the mouse brain. A red square indicates the pIII region. Right: confocal images of EGFP-labeled neurons in SD and RS mice at anterior posterior (AP) −3.8 mm. Blue, DAPI. Scale bar, 100 μm.

*(legend continued on next page)*

alpha (CALCA)-expressing neurons in the pIII region—the putative sleep center proposed by Mauthner—are preferentially active during NREM sleep. Activation of pIII CALCA neurons strongly promoted NREM sleep, and the effect is attributable at least partly to the glutamatergic subpopulation. In addition, cholecystokinin (CCK)-expressing glutamatergic neurons in the pIII region also promote NREM sleep, and they form local reciprocal connections with CALCA neurons. The rostral projections of both CALCA and CCK neurons to the POA and the caudal projection of CALCA neurons to the ventromedial medulla all promote NREM sleep, likely through their excitation of sleep-promoting neurons in those areas. Together, these results point to the pIII region as an excitatory sleep center where glutamatergic neurons promote NREM sleep through both local reciprocal connections and long-range projections to other sleep-promoting areas.

## RESULTS

### Identification of Sleep-Active Neurons in the pIII Region

Recovery sleep following several hours of sleep deprivation induces robust Fos expression in sleep-active neurons (Anaclet et al., 2012; Gong et al., 2004; Liu et al., 2017; Sherin et al., 1996; Zhang et al., 2015). To gain genetic access to the sleep-active neurons and to study their gene expression profiles, we crossed a $Fos^{CreER}$ transgenic mouse line that expresses tamoxifen-inducible Cre recombinase under the *Fos* promoter (Guenthner et al., 2013; Ye et al., 2016) with a Cre-dependent eGFP-L10a reporter line that expresses the EGFP-tagged ribosomal protein L10a (Long et al., 2014). In one group of crossed mice (n = 5), we paired an injection of 4 hydroxytamoxifen (4-OHT) with recovery sleep (RS; following 6 h of sleep deprivation). This allows the Cre estrogen receptor (CreER) expressed in sleep-active neurons to enter the nucleus, leading to permanent expression of EGFP-L10a (Figure 1A). In another group of mice (n = 5), we paired a 4-OHT injection with sleep deprivation (SD) to label wake-active neurons with EGFP-L10a.

We observed EGFP expression in multiple brain areas in both RS and SD mice (Table S1), but the number of labeled neurons differed between the two groups in several areas known to be involved in sleep-wake regulation (Figure S1A). For example, the tuberomammillary nucleus (TMN), VTA, parabrachial nucleus (PB), and *locus coeruleus* (LC) contained more EGFP-labeled neurons in SD mice, likely because of the abundance of wake-active neurons in those areas (Aston-Jones and Bloom, 1981; Eban-Rothschild et al., 2016; Kaur et al., 2017; Takahashi et al., 2006, 2010). In contrast, the parafacial zone (PZ), the lateral and dorsal paragigantocellular reticular nucleus (DPGi and LPGi, respectively), and the lateral preoptic area (LPO) showed more EGFP labeling in the RS group, likely because of the REM or NREM sleep-active neurons found in those regions (Anaclet et al., 2014; Chung et al., 2017; Verret et al., 2006; Weber et al., 2015; Zhang et al., 2015). Interestingly, the brain region with the highest relative expression in the RS group was the pIII (Figures 1B and S1A–S1C), the area originally proposed by Mauthner as a sleep center. This region contains the third oculomotor nucleus and the nearby Edinger-Westphal nucleus. Immunohistochemical staining confirmed strong Fos expression in the pIII region of RS mice, and comparison of Fos and EGFP expression demonstrated a high specificity (81.0% ± 2.3%, SEM) of EGFP labeling of sleep-active neurons (Figure S1D). Furthermore, very few EGFP-labeled neurons in RS mice expressed Fos following SD (11.4% ± 2.1%) and vice versa (3.2% ± 1.1%; Figure S1E), further demonstrating the specificity of EGFP labeling.

Fluorescence *in situ* hybridization (FISH) showed that most of the EGFP-labeled pIII neurons in the RS mice expressed the glutamatergic marker *Slc17a6* (encoding vGLUT2) or the cholinergic marker *Chat*, whereas none expressed the GABAergic marker *Slc32a1* (encoding vGAT) (Figure 1C). On the other hand, large fractions of glutamatergic (91.7% ± 1.3%, SEM) and cholinergic (87.8% ± 0.7%) neurons did not express EGFP. To identify more specific markers for the EGFP-labeled neurons, we performed gene expression profiling using translating ribosome affinity purification (Ekstrand et al., 2014; Heiman et al., 2008). The translating mRNA was isolated by immunoprecipitation (IP) of the EGFP-tagged L10a protein from tissue lysate using an anti-EGFP antibody. RNA sequencing (RNA-seq) revealed multiple genes significantly enriched in the EGFP-labeled neurons relative to the input RNAs (whole pIII lysate before immunoprecipitation) (Figure 1D; Table S2). In particular, we found three highly enriched neuropeptides: CALCA and calcitonin gene-related peptide beta (CALCB) together with galanin (GAL). Double FISH showed a more than 80% overlap between *Calca* and *Calcb* mRNAs (Figure 1E), indicating that the two closely related mRNAs are largely co-expressed in the pIII region. In contrast, *Gal* mRNA is expressed in a much smaller population of neurons, 53.2% of which also express *Calca* (Figure 1F). We thus focused on CALCA as a candidate marker. Double FISH of *EGFP* and *Calca* showed that 66.0% ± 1.5% (SEM) of EGFP-labeled pIII neurons in RS mice expressed *Calca* mRNA (Figure 1G), suggesting that CALCA could serve as an effective marker for sleep-active neurons.

(C) RS-EGFP neurons consist of glutamatergic and cholinergic subpopulations. Left: double fluorescence *in situ* hybridization (FISH) of EGFP and each neuronal marker. *Slc17a6*, vesicular glutamate transporter 2; *Chat*, choline acetyltransferase; *Slc32a1*, vesicular GABA transporter. Scale bar, 100 μm. Right: percentages of RS-EGFP neurons in the pIII region that express *Slc17a6*, *Chat*, or *Slc32a1*. Each circle indicates data from one mouse (n = 4 mice).

(D) Gene expression profiling of RS-EGFP neurons. Left: schematic of the experiment. Red square, brain region used for profiling. Right: volcano plot. Blue dot, L10a (Rpl10a) as a positive control. Orange dots, neuropeptide genes. *Calca*, calcitonin gene-related peptide alpha; *Calcb*, calcitonin gene-related peptide beta; *Gal*, galanin.

(E) Overlap between *Calca* and *Calcb* mRNA in the pIII region based on double FISH at AP −3.8 mm. Arrowheads indicate co-labeled neurons. Scale bar, 100 μm. The bar graph shows the percentages of *Calca* or *Calcb* neurons that are co-labeled. Each circle indicates data from one mouse (n = 4 mice).

(F) Similar to (E) for overlap between *Calca* and *Gal* (n = 5 mice).

(G) Overlap between RS-*EGFP* and *Calca* (n = 8 mice).

See also Figure S1 and Tables S1 and S2.

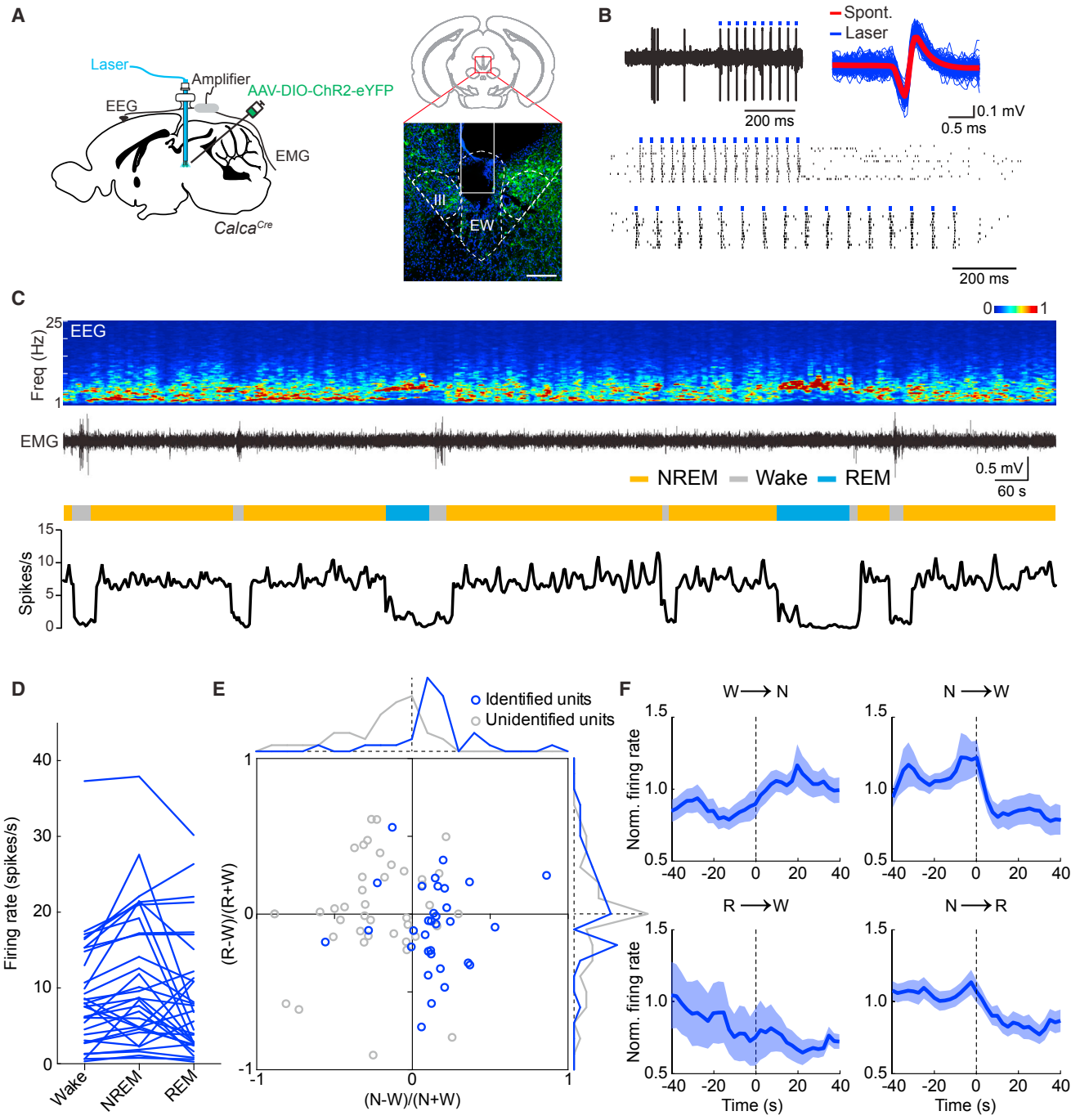


**Figure 2. CALCA Neurons in the pIII Region Are Preferentially Active during NREM Sleep**

(A) Schematic of optrode recording in freely moving mice. Right: fluorescence image of the pIII region (red box in the coronal diagram at AP −3.7 mm) in a *Calca*$^{Cre}$ mouse injected with AAV-EF1α-DIO-hChR2-eYFP.

(B) Example recording of spontaneous and laser-evoked spikes from an identified CALCA neuron. Top left: raw trace. Blue ticks, laser pulses. Top right: comparison of laser-evoked (blue) and averaged spontaneous (red) spike waveforms. Bottom: spike raster showing multiple laser stimulation trials at 15 and 30 Hz.

(C) Firing rate of an example CALCA neuron (bottom) together with an EEG spectrogram, EMG trace, and brain states (color coded). Freq., frequency.

(D) Firing rates of 32 identified CALCA neurons during different brain states. Each line shows the firing rates of one neuron.

(E) Firing rate modulation of all identified CALCA (blue, n = 32 neurons from 13 mice) and unidentified (gray, n = 40 neurons from 14 mice) neurons in the pIII region. Traces on the top and right show distributions of NREM-wake (top) and REM-wake (right) modulation for each population. The distributions of

*(legend continued on next page)*

## CALCA Neurons Are Preferentially Active during NREM Sleep

To directly measure the firing rates of pIII CALCA-expressing neurons across sleep and wake states, we tagged them with channelrhodopsin-2 (ChR2) and performed optrode recordings (Anikeeva et al., 2011; Xu et al., 2015; Figure 2A). A Cre-inducible adeno-associated virus (AAV) vector expressing ChR2 fused with enhanced yellow fluorescent protein (eYFP) was injected into the pIII region of a new line of *Calca*$^{Cre}$ mice (STAR Methods). During each recording session, high-frequency laser pulses (15 or 30 Hz, 10 ms per pulse, 16 pulses per train) were applied intermittently, and single units showing reliable laser-evoked spiking at short latencies and low jitter were identified as CALCA neurons (Figures 2B and S2). For each neuron, we recorded its endogenous activity (outside of laser stimulation periods) across multiple cycles of wake, REM, and NREM states, classified based on electroencephalogram (EEG) and electromyogram (EMG) recordings.

For the 32 identified CALCA neurons, the mean firing rate during NREM sleep was significantly higher than those during wakefulness ($p < 0.001$, Wilcoxon signed-rank test) and REM sleep ($p < 0.001$; Figures 2C–2E). Individually, 18 neurons showed significantly higher rates during NREM sleep than wakefulness ($p < 0.05$, Wilcoxon rank-sum test), and only 2 were significantly more active during wakefulness; 19 neurons showed significantly higher firing rates during NREM than REM sleep, and only 5 were more active during REM sleep (Table S3). The firing rates of CALCA neurons increased over ~15 s before onset of NREM sleep and decreased abruptly at the end of each NREM episode (Figure 2F), allowing them to participate in both the initiation and maintenance of NREM sleep. Compared with the identified CALCA neurons, the 40 unidentified pIII neurons showed a much higher degree of functional diversity, including many units that were more active during wakefulness or REM sleep (Figure 2E, gray symbols).

## CALCA Neurons in the pIII Region Promote NREM Sleep

Next, to test the causal role of CALCA neurons in sleep regulation, we bidirectionally manipulated their activity both optogenetically and chemogenetically. For optogenetic activation, laser stimulation (20 Hz, 2 min/trial) was applied randomly every 10–14 min in mice expressing ChR2 in their pIII CALCA neurons (Figure S3A). Activation of the CALCA neurons caused a strong increase in NREM sleep while suppressing both wakefulness and REM sleep (Figures 3A and 3B). Analysis of the probability of transitions between each pair of brain states showed that laser stimulation significantly enhanced wake → NREM and NREM → NREM transitions and decreased NREM → wake, wake → wake, and NREM → REM transitions (Figures S3C), indicating enhancement of both the initiation and maintenance of NREM sleep.

In *Calca*$^{Cre}$ mice expressing the light-activated chloride channel iC++ (Berndt et al., 2016) in the pIII region, laser stimulation (constant laser, 1 min/trial) strongly decreased NREM sleep and increased wakefulness (Figures 3C, 3D, and S3B). This was due to decreases in both wake → NREM and NREM → NREM transitions and increases in NREM → wake and wake → wake transitions (Figure S3D). In control mice expressing eYFP without ChR2 or iC++, laser stimulation had no effect (Figure S3E), and the changes in brain states induced by laser stimulation were significantly different between the ChR2 and control mice ($p < 0.0001$, bootstrap) and between iC++ and control mice ($p < 0.0001$).

We also tested the effects of chemogenetic manipulations of CALCA neurons (Sternson and Roth, 2014). For the activation experiment, AAV-EF1α-double-floxed inverse orientation (DIO)-hM3D(Gq)-mCherry was injected into the pIII region of *Calca*$^{Cre}$ mice. Compared with vehicle injection, clozapine-N-oxide (CNO) injection strongly increased NREM sleep and decreased wakefulness (Figure 3E). In contrast, in mice expressing AAV-EF1α-DIO-hM4D(Gi)-mCherry in their pIII CALCA neurons, CNO injection increased wakefulness and decreased sleep (Figure 3F). In control mice expressing mCherry without hM3D(Gq) or hM4D(Gi), CNO had no significant effect (Figure S3F).

To further assess the functional importance of pIII CALCA neurons, we ablated them by expressing a designer pro-caspase-3 (pro-taCasp3), whose activation causes apoptosis, and tobacco etch virus protease (TEVp), which activates pro-caspase-3 (Yang et al., 2013). Injection of AAV-EF1α-DIO-taCasp3-TEVp into the pIII region of *Calca*$^{Cre}$ mice caused a strong reduction in CALCA-expressing neurons (Figure S3G). Compared with their control littermates, mice with CALCA neuron ablation showed a marked decrease in NREM sleep during both the light and dark periods (Figure S3H). The NREM sleep reduction was even more pronounced during the recovery period following 5 h of sleep deprivation (Figure S3I). These results further support the functional importance of pIII CALCA neurons in NREM sleep generation.

## Functional Distinction between Glutamatergic and Cholinergic Neurons

Because the EGFP-labeled sleep-active population consists of both glutamatergic and cholinergic neurons (Figures 1C), we wondered whether CALCA-expressing neurons are similarly heterogeneous. FISH of *Slc17a6*, *Chat*, and *Calca* showed that the CALCA population indeed contains both glutamatergic (66.6% ± 0.6%, SEM) and cholinergic (35.9% ± 1.0%) neurons (with a small overlap between *Slc17a6* and *Chat* expression) (Figure 4A). This raises the question of whether the NREM-promoting effect of CALCA neurons is mediated by the glutamatergic or cholinergic subpopulation.

To test the function of cholinergic neurons, we injected Cre-inducible AAV-expressing ChR2-eYFP into *Chat*$^{Cre}$ mice (Rossi

NREM-wake modulation were significantly different between the identified and unidentified populations ($p < 0.001$, Kolmogorov-Smirnov test). W, wake; R, REM; NR, NREM.

(F) Mean firing rate of all identified CALCA neurons at brain state transitions (n = 32 neurons from 13 mice). The firing rate of each neuron was normalized by its mean during the whole recording session before being averaged across neurons. Time 0 indicates the transition point. Shading, ± SEM.

See also Figure S2 and Table S3.

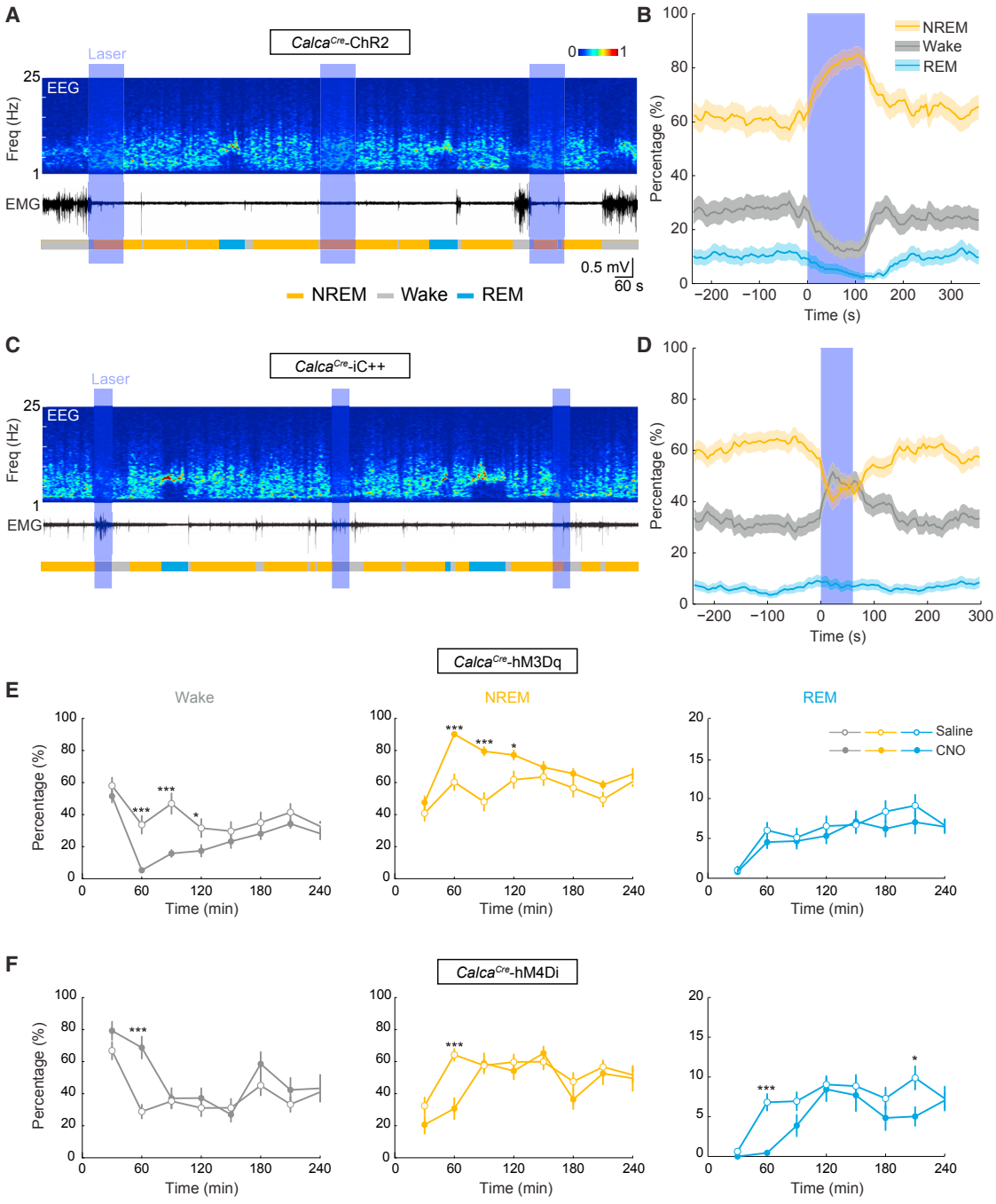


**Figure 3. Optogenetic and Chemogenetic Manipulations of pIII CALCA Neurons**

(A) An example optogenetic activation experiment in a *Calca*$^{Cre}$ mouse with AAV-EF1α-DIO-hChR2-eYFP injected into the pIII region. Shown are an EEG spectrogram, EMG trace, and brain states (color-coded). Blue stripe, laser stimulation period (20 Hz, 120 s).

(B) Percentage of time in the NREM, REM, or wake state before, during, and after laser activation of CALCA neurons, averaged from 8 mice. Shading, 95% confidence intervals (CIs). Blue stripe, laser stimulation period (20 Hz, 120 s). Laser stimulation significantly increased NREM sleep ($p < 0.0001$, bootstrap) and decreased wakefulness ($p < 0.0001$) and REM sleep ($p < 0.0001$).

(C) An example optogenetic inactivation experiment in a *Calca*$^{Cre}$ mouse with AAV-EF1α-DIO-iC++-eYFP injected into the pIII region. Blue stripe, laser stimulation (constant illumination, 60 s).

(D) Effect of optogenetic inactivation, averaged from 8 mice. Laser stimulation significantly decreased NREM sleep ($p < 0.0001$, bootstrap) and increased wakefulness ($p < 0.0001$).

*(legend continued on next page)*

et al., 2011). Optogenetic activation of cholinergic neurons (20 Hz, 2 min/trial) caused no significant change in any brain state ($p = 0.19$, 0.09, and 0.09 for wake, NREM, and REM states, respectively; Figure 4B). This was not due to ineffective activation of cholinergic neurons because, in a separate experiment, we found that even a brief laser stimulation (20 Hz, 4 s/trial) caused a strong reduction in pupil size (Figure 4D), likely because of activation of preganglionic cholinergic neurons in the Edinger-Westphal nucleus (Kozicz et al., 2011; McDougal and Gamlin, 2015). Although these cholinergic neurons may help to protect sleep from the awakening effect of visual stimulation through pupil constriction (Yuzgec et al., 2018), their optogenetic activation for a 2-min period appears to be insufficient to cause a significant increase in sleep. Conversely, despite the strong sleep-promoting effect of the CALCA neuron population (Figure 3), brief activation of these neurons had little effect on pupil size (Figure 4D), suggesting that pupil constriction requires the activation of some non-CALCA-expressing cholinergic neurons.

We then tested the function of pIII glutamatergic neurons by expressing ChR2 in *Slc17a6*$^{Cre}$ mice (Vong et al., 2011). Laser stimulation of the glutamatergic neurons at a low power (1 mW at the fiber tip) caused a strong increase in NREM sleep ($p < 0.0001$, bootstrap) and decreases in both wakefulness ($p < 0.0001$) and REM sleep ($p < 0.0001$; Figure 4C). Together with the effect of cholinergic neuron activation (Figure 4B), this suggests that the NREM-promoting effect of CALCA neurons is mediated largely by the glutamatergic subpopulation. It is important to note, however, that the effect of activation in *Slc17a6*$^{Cre}$ mice is sensitive to the laser power; at high power (3–5 mW), the stimulation increased wakefulness and decreased sleep (Figure S4A). This is very different from the effect of laser stimulation in *Calca*$^{Cre}$ mice, which promoted NREM sleep even at 10 mW (Figure S4B); this may be because some of the non-CALCA-expressing glutamatergic neurons outside of the pIII region promote wakefulness, and their activation at high laser power may override the sleep-promoting effect of pIII NREM neurons.

## CCK Neurons in the pIII Region Also Promote NREM Sleep

Although the majority of pIII CALCA neurons are glutamatergic, only a small fraction of glutamatergic neurons express CALCA (Figure 4A). Our observation that glutamatergic neuron activation at a low laser power enhanced NREM sleep (Figure 4C) raises the possibility that, besides the CALCA-expressing subpopulation, there are additional sleep-promoting glutamatergic neurons in the pIII region. Fos immunohistochemistry in RS mice (which labeled more sleep-active neurons than 4-OHT injection in the *Fos*$^{CreER}$ crossed with Cre-inducible EGFP-L10a mice) also showed that only 36.7% ± 4.3% of Fos-expressing neurons were CALCA cells (Figure S5A). Among the neuropeptides known to be expressed in sleep-promoting neurons in other brain regions (Chung et al., 2017), CCK is expressed in a population of pIII neurons. These CCK neurons are also glutamatergic but are distinct from the CALCA neurons (Figures 5A and 5B), and FOS immunohistochemistry in RS mice showed that 24.7% ± 1.8% of sleep-active neurons were CCK cells (Figure S5A).

To test the functional role of the CCK neurons, we injected a Cre-inducible AAV expressing ChR2 or iC++ into the pIII region of *Cck*$^{Cre}$ mice (Taniguchi et al., 2011). Optogenetic activation (20 Hz, 2 min/trial) of CCK neurons caused a significant increase in NREM sleep ($p < 0.0001$, bootstrap) and decreases in both wakefulness ($p < 0.0001$) and REM sleep ($p < 0.0001$; Figures 5C, S5B, and S5G) because of increases in both the initiation and maintenance of NREM sleep (Figure S5D). In contrast, optogenetic inactivation of these neurons (constant light, 1 min/trial) caused a significant decrease in NREM sleep and increase in wakefulness (Figures 5D, S5C, and S5E). In control mice expressing eYFP only, laser stimulation had no effect (Figures S5F), and the changes in brain states induced by laser stimulation were significantly different between ChR2 and control mice ($p < 0.0001$, bootstrap) and between iC++ and control mice ($p < 0.0001$). Thus, the CCK-expressing glutamatergic neurons in the pIII region also promote NREM sleep.

## Reciprocal Connections between CCK and CALCA Neurons

Given the spatial proximity between CCK and CALCA neurons, both of which promote NREM sleep, we wondered whether they interact with each other through local synaptic connections. To detect local inputs to CALCA neurons, we expressed an avian retroviral receptor (TVA) fused with mCherry (TC$^{66T}$) (Miyamichi et al., 2013) and a rabies glycoprotein (RG) by injecting two Cre-inducible AAV vectors (AAV2-CAG-FLEx-TC$^{66T}$ and AAV2-CAG-FLEx-RG) into the pIII region of *Calca*$^{Cre}$ mice. A modified rabies virus (RV) expressing EGFP (RV*dG*-EGFP+EnvA) was injected 3 weeks later to infect the TC$^{66T}$-expressing target neurons and to label their presynaptic inputs (Wickersham et al., 2007). Among the EGFP-labeled neurons in the pIII region, many expressed CCK (Figure 6A), indicating direct CCK → CALCA neuron connections. Conversely, the tracing experiment performed in *Cck*$^{Cre}$ mice revealed direct CALCA → CCK neuron connections (Figure 6B). In control mice injected with AAV-CAG-FLEx-TC$^{66T}$ and RV without AAV-CAG-FLEx-RG, we found no presynaptic neurons expressing EGFP without mCherry (Figures S6A and S6B), indicating specificity of transsynaptic RV labeling.

In addition to RV-mediated anatomical tracing, we also measured functional connections between CALCA and CCK neurons using electrophysiological recordings in acute brain slices. To measure CCK → CALCA neuron input, we injected AAV-DIO-ChR2-eYFP into the pIII region of *Cck*$^{Cre}$ mice. Whole-cell recordings were made in non-ChR2-expressing neurons, and cell types were identified using single-cell RT-PCR (Xu et al., 2015). As shown in Figures 6C and 6D, laser stimulation evoked excitatory postsynaptic potentials (EPSPs) in 11 of

(E) Chemogenetic activation experiment. Shown is the percentage of time in each brain state following CNO or vehicle injection in *Calca*$^{Cre}$ mice expressing hM3D(Gq). Horizontal axis, time after CNO/vehicle injection. Error bar, ± SEM; n = 5 mice. *$p < 0.05$, ***$p < 0.001$ (two-way ANOVA with Bonferroni correction).
(F) Chemogenetic inactivation experiment in *Calca*$^{Cre}$ mice expressing hM4D(Gi). n = 5 mice.
See also Figure S3.

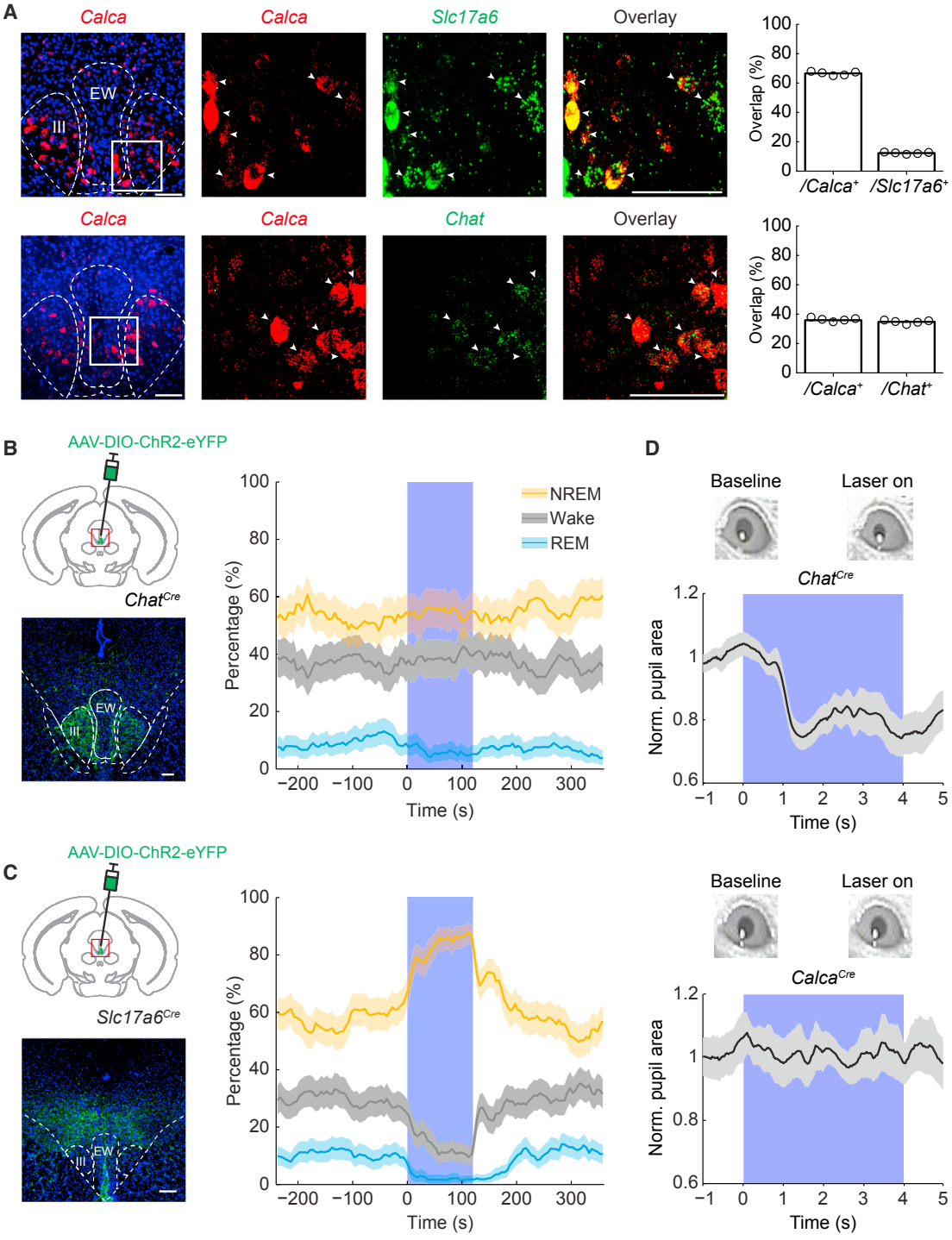


**Figure 4. Glutamatergic but Not Cholinergic pIII Neurons Promote NREM Sleep**

(A) Overlap between *Calca* and *Slc17a6* (top row) or *Chat* (bottom row) in the pIII region, measured by double FISH. Shown are coronal images at AP −3.8 mm. Arrowheads indicate co-labeled cells. Blue, DAPI. Scale bar, 100 μm. Right: percentages of *Calca*, *Slc17a6*, or *Chat* neurons that are co-labeled. Each circle indicates data from one mouse (n = 5 mice).

(B) Optogenetic activation of cholinergic pIII neurons did not affect sleep. Left: fluorescence image of the pIII region (red box in the coronal diagram at AP −3.8 mm) in a $Chat^{Cre}$ mouse injected with AAV-EF1α-DIO-hChR2-eYFP. Blue, DAPI. Scale bar, 100 μm. Right: percentage of time in the NREM, REM, or wake state before, during, and after laser stimulation, averaged from 4 mice. Shading, 95% CI. Blue stripe, laser stimulation period (20 Hz, 120 s).

*(legend continued on next page)*

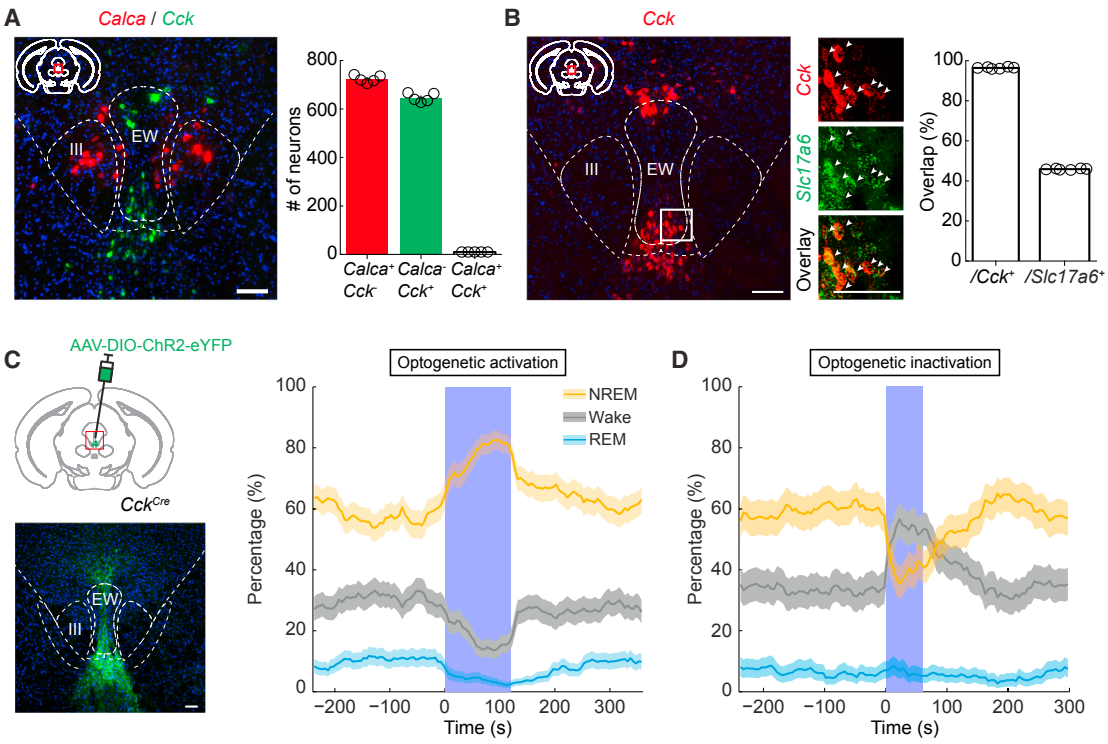


**Figure 5. CCK Neurons in the pIII Region Promote NREM Sleep**

(A) CCK and CALCA neurons are distinct populations in the pIII region. Left: fluorescence image showing double FISH of *Calca* and *Cck* in the pIII region (red box in the coronal diagram at AP −3.8 mm). Blue, DAPI. Scale bar, 100 μm. Right: number of neurons expressing *Calca*, *Cck*, or both. Each circle indicates data from one mouse (n = 5 mice).

(B) CCK neurons are glutamatergic. Left: double FISH of *Cck* and *Slc17a6* in the pIII region (red box in the coronal diagram at AP −3.8 mm). Scale bar, 100 μm. Right: percentage of *Cck*- or *Slc17a6*-expressing neurons that are co-labeled. Each circle indicates data from one mouse (n = 6 mice).

(C) Optogenetic activation of CCK neurons promotes NREM sleep. Left: fluorescence image of the pIII region (red box in the coronal diagram at AP −3.8 mm) in a $Cck^{Cre}$ mouse injected with AAV-EF1α-DIO-hChR2-eYFP. Scale bar, 100 μm. Right: percentage of time in the NREM, REM, or wake state before, during, and after laser stimulation, averaged from 8 mice. Shading, 95% CI. Blue stripe, laser stimulation period (20 Hz, 120 s). Laser stimulation significantly increased NREM sleep ($p < 0.0001$, bootstrap) and decreased wakefulness ($p < 0.0001$) and REM sleep ($p < 0.0001$).

(D) Similar to (C) but for optogenetic inactivation of CCK neurons (n = 6 mice). Laser stimulation significantly decreased NREM sleep ($p < 0.0001$, bootstrap) and increased wakefulness ($p < 0.0001$). Blue stripe, laser stimulation period (constant illumination, 60 s).

See also Figure S5.

15 glutamatergic CALCA neurons, which were blocked by the α-amino-3-hydroxy-5-methyl-4-isoxazolepropionic acid (AMPA) receptor antagonist cyanquixaline (CNQX), confirming functional CCK → CALCA neuron excitation. Conversely, in $Calca^{Cre}$ mice injected with AAV-DIO-ChR2-eYFP, laser stimulation evoked glutamatergic EPSPs in 7 of 12 CCK neurons (Figures 6E and 6F), demonstrating CALCA → CCK neuron excitation.

Together, these anatomical and electrophysiological experiments indicate that CCK- and CALCA-expressing neurons are reciprocally connected within the pIII region. Reciprocal excitation between neuronal populations could serve to reinforce and stabilize their activation, making the activity pattern resistant to small perturbations or noise (Wang, 2009). Because both CCK and CALCA pIII neurons promote NREM sleep, the reciprocal excitation between them could contribute to the stability of NREM sleep.

## Long-Range Projections of CALCA and CCK Neurons

Finally, we examined the long-range projections of CALCA and CCK neurons. Both populations of pIII neurons project rostrally and arborize extensively in the POA, a prominent sleep-promoting brain area (von Economo, 1930; Lu et al., 2000; McGinty and Sterman, 1968; Nauta, 1946; Sallanon et al., 1989; Zhang et al., 2015). To test the functional role of the POA projection from CCK neurons, we injected AAV-DIO-ChR2-eYFP into the pIII region of $Cck^{Cre}$ mice and inserted an optic fiber into the POA. Activation

(C) Similar to (B) but in $Slc17a6^{Cre}$ mice (n = 6 mice). Shown is a coronal image at AP −3.7 mm. Laser stimulation significantly increased NREM sleep ($p < 0.0001$, bootstrap) and decreased wakefulness ($p < 0.0001$) and REM sleep ($p < 0.0001$).

(D) Optogenetic activation of cholinergic (top) but not CALCA-expressing (bottom) pIII neurons caused pupil constriction. For each trial, the pupil area was normalized by its mean over the 2 s before laser stimulation. Shading, ± SEM. Blue stripe, laser stimulation period (20 Hz, 4 s).

See also Figure S4.

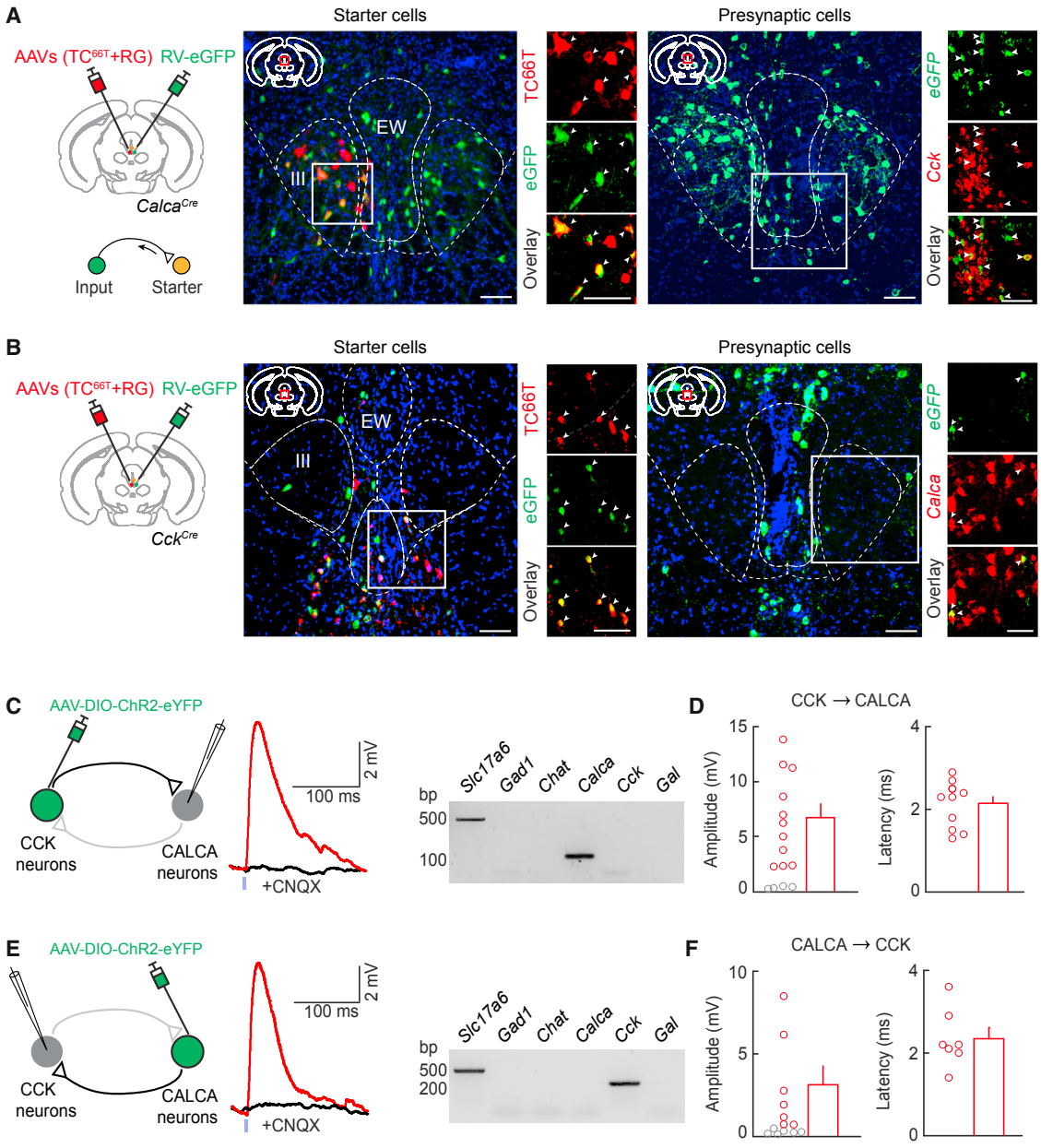


**Figure 6. CCK and CALCA Neurons Form Reciprocal Connections**

(A) Monosynaptic innervation of CALCA neurons by CCK neurons. Left: fluorescence image (at AP −3.8 mm) of starter cells in the pIII region (expressing both EGFP and mCherry, indicated by arrowheads). Right: fluorescence image (at AP −3.8 mm) of double FISH of *EGFP* and *Cck*. The regions in the white boxes are shown on the right. Arrowheads indicate co-labeled neurons. Blue, DAPI. Scale bars, 100 μm.

(B) Similar to (A) for innervation of CCK neurons by CALCA neurons. The coronal images are at AP −3.9 mm (left) and −3.8 mm (right).

(C) CCK → CALCA neuron connections measured electrophysiologically. Left: schematic of slice recording. Center, light-evoked excitatory postsynaptic potential (EPSP) in an example CALCA neuron (red, recorded under current clamp), which was blocked by CNQX (20 μM, black). Blue tick, laser stimulus. Right: single-cell RT-PCR identification of the recorded CALCA neuron, which also expressed *Slc17a6*.

(D) Population summary of EPSP amplitude and latency. Red circles, cells with significant responses ($p < 0.05$, t test). Gray circles, cells with no significant response. Bar, mean ± SEM.

(E and F) Similar to (C) and (D) for CALCA → CCK neuron connections.

See also Figure S6.

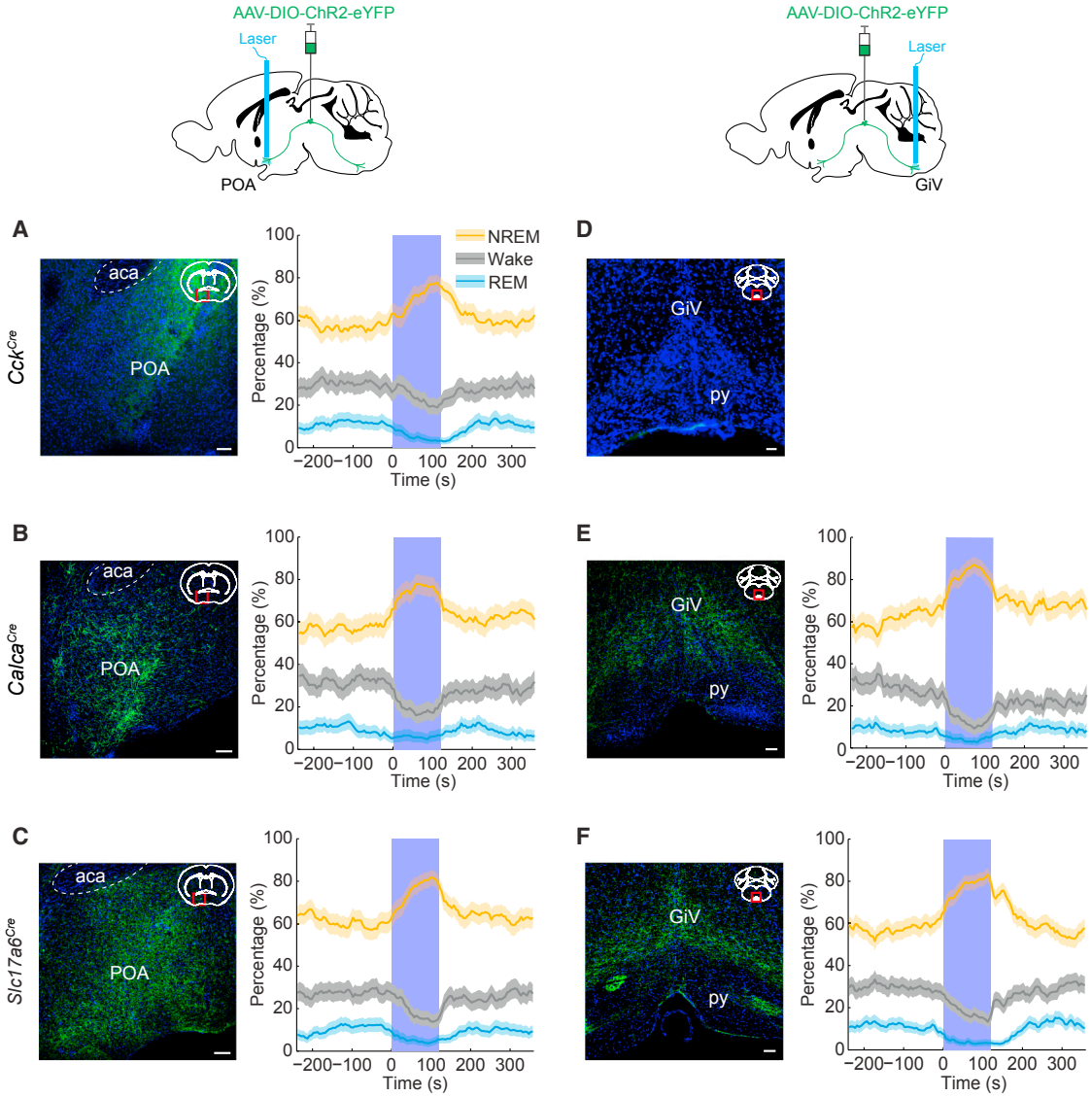


**Figure 7. Rostral and Caudal Projections of pIII Neurons Promote NREM Sleep**

(A) Optogenetic activation of CCK neuron axons in the POA promotes NREM sleep. Left: fluorescence image of POA (red box in the coronal diagram) in a *Cck*$^{Cre}$ mouse injected with AAV-DIO-ChR2-eYFP into the pIII. Blue, DAPI. POA, preoptic area; aca, anterior commissure. Scale bar, 100 μm. Right: percentage of time in the NREM, REM, or wake state before, during, and after laser stimulation, averaged from 5 mice. Shading, 95% CI. Blue stripe, laser stimulation period (20 Hz, 120 s). Laser stimulation significantly increased NREM sleep ($p < 0.0001$, bootstrap) and decreased wakefulness ($p < 0.0001$) and REM sleep ($p < 0.0001$).

(B) Similar to (A) for optogenetic activation of CALCA neuron axons in the POA (n = 5 mice). Laser stimulation significantly increased NREM sleep ($p < 0.0001$, bootstrap) and decreased wakefulness ($p < 0.0001$).

(C) Similar to (A) for optogenetic activation of glutamatergic neuron axons in the POA of *Slc17a6*$^{Cre}$ mice (n = 5 mice). Laser stimulation significantly increased NREM sleep ($p < 0.0001$, bootstrap) and decreased wakefulness ($p < 0.0001$) and REM sleep ($p < 0.0001$).

(D) Fluorescence image of the posterior ventromedial medulla (red box in coronal diagram) in a *Cck*$^{Cre}$ mouse injected with AAV-DIO-ChR2-eYFP in the pIII region, showing no projection from CCK neurons to the posterior ventromedial medulla. py, pyramidal tract. GiV, gigantocellular reticular nucleus.

(E) Optogenetic activation of CALCA neuron axons in the posterior ventromedial medulla; n = 5 mice. Laser stimulation significantly increased NREM sleep ($p < 0.0001$, bootstrap) and decreased wakefulness ($p < 0.0001$).

(F) Similar to (E) for optogenetic activation of glutamatergic neuron axons in the posterior ventromedial medulla; n = 5 mice. Laser stimulation significantly increased NREM sleep ($p < 0.0001$, bootstrap) and decreased wakefulness ($p < 0.0001$) and REM sleep ($p < 0.0001$).

See also Figure S7.

of CCK neuron axons increased NREM sleep at the expense of both wakefulness and REM sleep (Figure 7A; $p < 0.0001$). Other than the POA, the main projection targets of pIII CCK neurons are the lateral hypothalamus (LH) and lateral septum (LS) (Figure S7A). However, laser stimulation had no significant effect in either the LH ($p = 0.38$, 0.37, and 0.21 for wake, NREM, and

REM states, respectively) or the LS ($p = 0.34$, 0.42, and 0.41), indicating that the POA projection is particularly important for sleep regulation by pIII CCK neurons.

Activation of CALCA neuron axons in the POA also caused a strong increase in NREM sleep and decrease in wakefulness (Figure 7B; $p < 0.0001$, bootstrap). Similar effects were induced by activating the POA projection in *Slc17a6*$^{Cre}$ mice (Figure 7C). In contrast, we found no POA projection from cholinergic or galaninergic pIII neurons (Figures S7C and S7D), indicating that the effect of activating CALCA neuron axons (Figure 7B) is caused by the glutamatergic subset. Optogenetic stimulation of axon terminals could, in principle, evoke antidromic spiking and activation of other collateral projections. We thus tested the effect of local chemogenetic activation, which causes slow depolarization of axon terminals through G protein-coupled signaling and is unlikely to induce antidromic spiking (Forcelli, 2017). In *Calca*$^{Cre}$ mice injected with AAV-DIO-hM3D(Gq)-mCherry in the pIII region, local CNO injection in the POA caused a significant increase in NREM sleep (Figure S7E), further demonstrating a contribution of the POA projection to sleep regulation.

CALCA but not CCK neurons also project caudally, arborizing extensively in the posterior ventromedial medulla (Figures 7D and 7E). Activating the CALCA neuron axons in this region also increased NREM sleep and decreased wakefulness (Figure 7E; $p < 0.0001$). Similar effects were observed by activating the pIII → medulla projection in *Slc17a6*$^{Cre}$ mice (Figure 7F). Interestingly, dual retrograde tracing showed that the pIII glutamatergic neurons projecting to the ventromedial medulla and the POA are largely separate populations (Figure S7G), indicating that, even with antidromic spiking, the NREM increase induced by medulla stimulation is unlikely mediated by the POA projection and vice versa. Local chemogenetic activation of CALCA neuron terminals in the medulla also caused a significant increase in NREM sleep (Figure S7F), further supporting the contribution of this projection. In addition to the POA and medulla, pIII CALCA neurons also project to the medial vestibular nucleus (MV) and LH (Figure S7B). Optogenetic stimulation of CALCA neuron terminals in the MV had no significant effect ($p = 0.18$, 0.15, and 0.48 for wake, NREM, and REM states, respectively). Although stimulation in the LH caused an increase in NREM sleep ($p = 0.006$), the magnitude of the increase was significantly lower than those induced by POA ($p < 0.0001$, bootstrap) or medulla ($p < 0.0001$) stimulation. Together, these results indicate that the POA and medulla projections from pIII CALCA neurons are particularly important for NREM sleep generation.

## DISCUSSION

Using activity-dependent labeling, gene profiling, optrode recording, and bidirectional optogenetic and chemogenetic manipulations, we identified two interconnected populations of excitatory sleep neurons in the midbrain. Although the CCK-expressing population is almost entirely glutamatergic (Figure 5B), the CALCA population contains both glutamatergic and cholinergic neurons (Figure 4A). The NREM-promoting effect, however, is at least partly attributable to the glutamatergic subpopulation (Figures 4B and 4C). In addition to their reciprocal connections within the pIII region (Figure 6), both CALCA and CCK neurons send long-range projections to other brain regions, including the well-known sleep-promoting area POA. Activation of both the rostral and caudal projections promoted NREM sleep (Figure 7), indicating multiple downstream pathways mediating the effect.

Cholinergic neurons in the Edinger-Westphal nucleus in the pIII region are known to control pupil constriction through their projection to the parasympathetic ciliary ganglion (Kozicz et al., 2011; McDougal and Gamlin, 2015; Yuzgec et al., 2018). The pupil size is tightly coupled to the animal's brain state, and it is greatly reduced during drowsiness and sleep (McGinley et al., 2015; Reimer et al., 2014, 2016; Vinck et al., 2015; Yuzgec et al., 2018). This implies that preganglionic cholinergic neurons are active during sleep and that they may correspond to the EGFP-labeled cholinergic population in RS mice (Figure 1C). These cholinergic neurons may share common inputs with sleep-active glutamatergic neurons or even receive input from the glutamatergic population. The pupil constriction caused by their activation could, in turn, contribute to sleep stabilization by gating visual inputs (Yuzgec et al., 2018). It is interesting to note that Mauthner originally proposed the pIII region as a sleep center partly because of the oculomotor changes associated with natural sleep. In future studies, it would be of great interest to characterize the interactions between neurons controlling sleep versus oculomotor functions.

Given the effects of CALCA neuron activation (Figure 3), the NREM-promoting effect of CCK neurons could be partly mediated by the CCK → CALCA connection (Figures 6A and 6C). Conversely, the NREM-promoting function of CALCA neurons could be partly mediated by the CALCA → CCK pathway (Figures 6B and 6D). These reciprocal connections could serve to stabilize the activation of both populations during sleep. Both CALCA and CCK neurons project to the POA (Figures 7A and 7B), which contains a large number of GABAergic sleep-active neurons (Chung et al., 2017; Gong et al., 2004; McGinty and Sterman, 1968; Sherin et al., 1996; Takahashi et al., 2009; Zhang et al., 2015). The sleep-promoting effect of pIII glutamatergic neurons is likely to involve their excitation of POA sleep neurons. The caudal projection of CALCA neurons to the posterior ventromedial medulla promotes NREM sleep as well (Figure 7E), although the downstream target neurons mediating the effect remain to be identified. In RS and SD mice, there were similar numbers of EGFP-labeled neurons in this region (Figure S1A; Table S1), suggesting intermingled sleep- and wake-active neurons. Besides the CALCA and CCK populations, there may be additional NREM-promoting glutamatergic neurons in the midbrain. The recurrent local connections among these neurons could help to stabilize their activation during sleep, whereas the divergent long-range projections may serve to coordinate the global transition from wakefulness to sleep across multiple brain regions.

## STAR★METHODS

Detailed methods are provided in the online version of this paper and include the following:

- KEY RESOURCES TABLE
- CONTACT FOR REAGENT AND RESOURCE SHARING

- EXPERIMENTAL MODEL AND SUBJECT DETAILS
- METHOD DETAILS
  - Virus Preparation
  - Surgical Procedures
  - Polysomnographic Recordings
  - Sleep Deprivation and Sleep Rebound Experiment
  - Optrode Recording
  - Optogenetic Manipulation
  - Chemogenetic Manipulation
  - Pupillometry
  - Slice Recording
  - Single-Cell RT-PCR
  - Immunohistochemistry and Fluorescence *in situ* Hybridization (FISH)
  - Translating Ribosome Affinity Purification
- QUANTIFICATION AND STATISTICAL ANALYSIS
- DATA AND SOFTWARE AVAILABILITY
  - Data Resources


## SUPPLEMENTAL INFORMATION

Supplemental Information can be found online at https://doi.org/10.1016/j.cell.2019.03.041.

## ACKNOWLEDGMENTS

We thank M. Xu and K. Chen for providing programs for data analysis; C. Ma and W. Chang for sharing the virus for the rabies virus tracing experiment; and S. Tsang, K. Kafer, and M. Chiang for help with generating and maintaining the new *Calca*$^{Cre}$ mouse line. This work was supported by the Howard Hughes Medical Institute.

## AUTHOR CONTRIBUTIONS

Z.Z. and Y.D. designed the study and wrote the paper. Z.Z. and P.Z. performed most of the experiments. F.H. performed the pupillometry experiment. Z.B., S.L., and F.W. wrote the programs for data analysis. Y.R. performed part of the FISH experiment. X.D. performed part of the single-cell RT-PCR experiment. S.C. performed part of the TRAP experiment. R.D.P. provided the new *Calca*$^{Cre}$ mouse line and helped edit the paper. Y.D. supervised all aspects of the work.

## DECLARATION OF INTERESTS

The authors declare no competing interests.

Received: July 10, 2018
Revised: January 4, 2019
Accepted: March 20, 2019
Published: April 25, 2019

## REFERENCES

Alam, M.A., Kumar, S., McGinty, D., Alam, M.N., and Szymusiak, R. (2014). Neuronal activity in the preoptic hypothalamus during sleep deprivation and recovery sleep. J. Neurophysiol. *111*, 287–299.

Anaclet, C., Lin, J.S., Vetrivelan, R., Krenzer, M., Vong, L., Fuller, P.M., and Lu, J. (2012). Identification and characterization of a sleep-active cell group in the rostral medullary brainstem. J. Neurosci. *32*, 17970–17976.

Anaclet, C., Ferrari, L., Arrigoni, E., Bass, C.E., Saper, C.B., Lu, J., and Fuller, P.M. (2014). The GABAergic parafacial zone is a medullary slow wave sleep-promoting center. Nat. Neurosci. *17*, 1217–1224.

Anikeeva, P., Andalman, A.S., Witten, I., Warden, M., Goshen, I., Grosenick, L., Gunaydin, L.A., Frank, L.M., and Deisseroth, K. (2011). Optetrode: a multichannel readout for optogenetic control in freely moving mice. Nat. Neurosci. *15*, 163–170.

Aston-Jones, G., and Bloom, F.E. (1981). Activity of norepinephrine-containing locus coeruleus neurons in behaving rats anticipates fluctuations in the sleep-waking cycle. J. Neurosci. *1*, 876–886.

Berndt, A., Lee, S.Y., Wietek, J., Ramakrishnan, C., Steinberg, E.E., Rashid, A.J., Kim, H., Park, S., Santoro, A., Frankland, P.W., et al. (2016). Structural foundations of optogenetics: Determinants of channelrhodopsin ion selectivity. Proc. Natl. Acad. Sci. USA *113*, 822–829.

Carter, M.E., Soden, M.E., Zweifel, L.S., and Palmiter, R.D. (2013). Genetic identification of a neural circuit that suppresses appetite. Nature *503*, 111–114.

Chung, S., Weber, F., Zhong, P., Tan, C.L., Nguyen, T.N., Beier, K.T., Hörmann, N., Chang, W.C., Zhang, Z., Do, J.P., et al. (2017). Identification of preoptic sleep neurons using retrograde labelling and gene profiling. Nature *545*, 477–481.

Eban-Rothschild, A., Rothschild, G., Giardino, W.J., Jones, J.R., and de Lecea, L. (2016). VTA dopaminergic neurons regulate ethologically relevant sleep-wake behaviors. Nat. Neurosci. *19*, 1356–1366.

Ekstrand, M.I., Nectow, A.R., Knight, Z.A., Latcha, K.N., Pomeranz, L.E., and Friedman, J.M. (2014). Molecular profiling of neurons based on connectivity. Cell *157*, 1230–1242.

Foley, P.B. (2018). Encephalitis Lethargica: The Mind and Brain Virus (Springer).

Forcelli, P.A. (2017). Applications of optogenetic and chemogenetic methods to seizure circuits: Where to go next? J. Neurosci. Res. *95*, 2345–2356.

Gong, H., McGinty, D., Guzman-Marin, R., Chew, K.T., Stewart, D., and Szymusiak, R. (2004). Activation of c-fos in GABAergic neurones in the preoptic area during sleep and in response to sleep deprivation. J. Physiol. *556*, 935–946.

Guenthner, C.J., Miyamichi, K., Yang, H.H., Heller, H.C., and Luo, L. (2013). Permanent genetic access to transiently active neurons via TRAP: targeted recombination in active populations. Neuron *78*, 773–784.

Harding, E.C., Yu, X., Miao, A., Andrews, N., Ma, Y., Ye, Z., Lignos, L., Miracca, G., Ba, W., Yustos, R., et al. (2018). A Neuronal Hub Binding Sleep Initiation and Body Cooling in Response to a Warm External Stimulus. Curr. Biol. *28*, 2263–2273.e4.

Hassani, O.K., Lee, M.G., and Jones, B.E. (2009). Melanin-concentrating hormone neurons discharge in a reciprocal manner to orexin neurons across the sleep-wake cycle. Proc. Natl. Acad. Sci. USA *106*, 2418–2422.

Hauswirth, W.W., Lewin, A.S., Zolotukhin, S., and Muzyczka, N. (2000). Production and purification of recombinant adeno-associated virus. Methods Enzymol. *316*, 743–761.

Heiman, M., Schaefer, A., Gong, S., Peterson, J.D., Day, M., Ramsey, K.E., Suárez-Fariñas, M., Schwarz, C., Stephan, D.A., Surmeier, D.J., et al. (2008). A translational profiling approach for the molecular characterization of CNS cell types. Cell *135*, 738–748.

Heiman, M., Kulicke, R., Fenster, R.J., Greengard, P., and Heintz, N. (2014). Cell type-specific mRNA purification by translating ribosome affinity purification (TRAP). Nat. Protoc. *9*, 1282–1291.

Jego, S., Glasgow, S.D., Herrera, C.G., Ekstrand, M., Reed, S.J., Boyce, R., Friedman, J., Burdakov, D., and Adamantidis, A.R. (2013). Optogenetic identification of a rapid eye movement sleep modulatory circuit in the hypothalamus. Nat. Neurosci. *16*, 1637–1643.

Kaur, S., Wang, J.L., Ferrari, L., Thankachan, S., Kroeger, D., Venner, A., Lazarus, M., Wellman, A., Arrigoni, E., Fuller, P.M., et al. (2017). A genetically defined circuit for arousal from sleep during hypercapnia. Neuron *96*, 1153–1167.e5.

Knight, Z.A., Tan, K., Birsoy, K., Schmidt, S., Garrison, J.L., Wysocki, R.W., Emiliano, A., Ekstrand, M.I., and Friedman, J.M. (2012). Molecular profiling of activated neurons by phosphorylated ribosome capture. Cell *151*, 1126–1137.

Konadhode, R.R., Pelluru, D., Blanco-Centurion, C., Zayachkivsky, A., Liu, M., Uhde, T., Glen, W.B., Jr., van den Pol, A.N., Mulholland, P.J., and Shiromani, P.J. (2013). Optogenetic stimulation of MCH neurons increases sleep. J. Neurosci. *33*, 10257–10263.

Kozicz, T., Bittencourt, J.C., May, P.J., Reiner, A., Gamlin, P.D., Palkovits, M., Horn, A.K., Toledo, C.A., and Ryabinin, A.E. (2011). The Edinger-Westphal nucleus: a historical, structural, and functional perspective on a dichotomous terminology. J. Comp. Neurol. *519*, 1413–1434.

Lambolez, B., Audinat, E., Bochet, P., Crépel, F., and Rossier, J. (1992). AMPA receptor subunits expressed by single Purkinje cells. Neuron *9*, 247–258.

Li, B., and Dewey, C.N. (2011). RSEM: accurate transcript quantification from RNA-Seq data with or without a reference genome. BMC Bioinformatics *12*, 323.

Liu, K., Kim, J., Kim, D.W., Zhang, Y.S., Bao, H., Denaxa, M., Lim, S.A., Kim, E., Liu, C., Wickersham, I.R., et al. (2017). Lhx6-positive GABA-releasing neurons of the zona incerta promote sleep. Nature *548*, 582–587.

Long, J.Z., Svensson, K.J., Tsai, L., Zeng, X., Roh, H.C., Kong, X., Rao, R.R., Lou, J., Lokurkar, I., Baur, W., et al. (2014). A smooth muscle-like origin for beige adipocytes. Cell Metab. *19*, 810–820.

Lu, J., Greco, M.A., Shiromani, P., and Saper, C.B. (2000). Effect of lesions of the ventrolateral preoptic nucleus on NREM and REM sleep. J. Neurosci. *20*, 3830–3842.

McDougal, D.H., and Gamlin, P.D. (2015). Autonomic control of the eye. Compr. Physiol. *5*, 439–473.

McGinley, M.J., David, S.V., and McCormick, D.A. (2015). Cortical membrane potential signature of optimal states for sensory signal detection. Neuron *87*, 179–192.

McGinty, D.J., and Sterman, M.B. (1968). Sleep suppression after basal forebrain lesions in the cat. Science *160*, 1253–1255.

Miyamichi, K., Shlomai-Fuchs, Y., Shu, M., Weissbourd, B.C., Luo, L., and Mizrahi, A. (2013). Dissecting local circuits: parvalbumin interneurons underlie broad feedback control of olfactory bulb output. Neuron *80*, 1232–1245.

Nauta, W.J. (1946). Hypothalamic regulation of sleep in rats; an experimental study. J. Neurophysiol. *9*, 285–316.

Nectow, A.R., Ekstrand, M.I., and Friedman, J.M. (2015). Molecular characterization of neuronal cell types based on patterns of projection with Retro-TRAP. Nat. Protoc. *10*, 1319–1327.

Oishi, Y., Xu, Q., Wang, L., Zhang, B.J., Takahashi, K., Takata, Y., Luo, Y.J., Cherasse, Y., Schiffmann, S.N., de Kerchove d'Exaerde, A., et al. (2017). Slow-wave sleep is controlled by a subset of nucleus accumbens core neurons in mice. Nat. Commun. *8*, 734.

Osakada, F., and Callaway, E.M. (2013). Design and generation of recombinant rabies virus vectors. Nat. Protoc. *8*, 1583–1601.

Reimer, J., Froudarakis, E., Cadwell, C.R., Yatsenko, D., Denfield, G.H., and Tolias, A.S. (2014). Pupil fluctuations track fast switching of cortical states during quiet wakefulness. Neuron *84*, 355–362.

Reimer, J., McGinley, M.J., Liu, Y., Rodenkirch, C., Wang, Q., McCormick, D.A., and Tolias, A.S. (2016). Pupil fluctuations track rapid changes in adrenergic and cholinergic activity in cortex. Nat. Commun. *7*, 13289.

Rossi, J., Balthasar, N., Olson, D., Scott, M., Berglund, E., Lee, C.E., Choi, M.J., Lauzon, D., Lowell, B.B., and Elmquist, J.K. (2011). Melanocortin-4 receptors expressed by cholinergic neurons regulate energy balance and glucose homeostasis. Cell Metab. *13*, 195–204.

Sallanon, M., Denoyer, M., Kitahama, K., Aubert, C., Gay, N., and Jouvet, M. (1989). Long-lasting insomnia induced by preoptic neuron lesions and its transient reversal by muscimol injection into the posterior hypothalamus in the cat. Neuroscience *32*, 669–683.

Sherin, J.E., Shiromani, P.J., McCarley, R.W., and Saper, C.B. (1996). Activation of ventrolateral preoptic neurons during sleep. Science *271*, 216–219.

Sternson, S.M., and Roth, B.L. (2014). Chemogenetic tools to interrogate brain functions. Annu. Rev. Neurosci. *37*, 387–407.

Szymusiak, R., Alam, N., Steininger, T.L., and McGinty, D. (1998). Sleep-waking discharge patterns of ventrolateral preoptic/anterior hypothalamic neurons in rats. Brain Res. *803*, 178–188.

Takahashi, K., Lin, J.S., and Sakai, K. (2006). Neuronal activity of histaminergic tuberomammillary neurons during wake-sleep states in the mouse. J. Neurosci. *26*, 10292–10298.

Takahashi, K., Lin, J.S., and Sakai, K. (2009). Characterization and mapping of sleep-waking specific neurons in the basal forebrain and preoptic hypothalamus in mice. Neuroscience *161*, 269–292.

Takahashi, K., Kayama, Y., Lin, J.S., and Sakai, K. (2010). Locus coeruleus neuronal activity during the sleep-waking cycle in mice. Neuroscience *169*, 1115–1126.

Taniguchi, H., He, M., Wu, P., Kim, S., Paik, R., Sugino, K., Kvitsiani, D., Fu, Y., Lu, J., Lin, Y., et al. (2011). A resource of Cre driver lines for genetic targeting of GABAergic neurons in cerebral cortex. Neuron *71*, 995–1013.

Tervo, D.G., Hwang, B.Y., Viswanathan, S., Gaj, T., Lavzin, M., Ritola, K.D., Lindo, S., Michael, S., Kuleshova, E., Ojala, D., et al. (2016). A designer AAV variant permits efficient retrograde access to projection neurons. Neuron *92*, 372–382.

Tsunematsu, T., Ueno, T., Tabuchi, S., Inutsuka, A., Tanaka, K.F., Hasuwa, H., Kilduff, T.S., Terao, A., and Yamanaka, A. (2014). Optogenetic manipulation of activity and temporally controlled cell-specific ablation reveal a role for MCH neurons in sleep/wake regulation. J. Neurosci. *34*, 6896–6909.

Verret, L., Fort, P., Gervasoni, D., Léger, L., and Luppi, P.H. (2006). Localization of the neurons active during paradoxical (REM) sleep and projecting to the locus coeruleus noradrenergic neurons in the rat. J. Comp. Neurol. *495*, 573–586.

Vinck, M., Batista-Brito, R., Knoblich, U., and Cardin, J.A. (2015). Arousal and locomotion make distinct contributions to cortical activity patterns and visual encoding. Neuron *86*, 740–754.

von Economo, C. (1930). Sleep as a problem of localization. J. Nerv. Ment. Dis. *71*, 249–259.

Vong, L., Ye, C., Yang, Z., Choi, B., Chua, S., Jr., and Lowell, B.B. (2011). Leptin action on GABAergic neurons prevents obesity and reduces inhibitory tone to POMC neurons. Neuron *71*, 142–154.

Wang, X.-J. (2009). Attractor Network Models. In Encyclopedia of Neuroscience, L.R. Squire, ed. (Elsevier), pp. 667–679.

Weber, F., Chung, S., Beier, K.T., Xu, M., Luo, L., and Dan, Y. (2015). Control of REM sleep by ventral medulla GABAergic neurons. Nature *526*, 435–438.

Weber, F., Hoang Do, J.P., Chung, S., Beier, K.T., Bikov, M., Saffari Doost, M., and Dan, Y. (2018). Regulation of REM and Non-REM sleep by periaqueductal GABAergic neurons. Nat. Commun. *9*, 354.

Wickersham, I.R., Lyon, D.C., Barnard, R.J., Mori, T., Finke, S., Conzelmann, K.K., Young, J.A., and Callaway, E.M. (2007). Monosynaptic restriction of transsynaptic tracing from single, genetically targeted neurons. Neuron *53*, 639–647.

Xu, M., Chung, S., Zhang, S., Zhong, P., Ma, C., Chang, W.C., Weissbourd, B., Sakai, N., Luo, L., Nishino, S., and Dan, Y. (2015). Basal forebrain circuit for sleep-wake control. Nat. Neurosci. *18*, 1641–1647.

Yang, C.F., Chiang, M.C., Gray, D.C., Prabhakaran, M., Alvarado, M., Juntti, S.A., Unger, E.K., Wells, J.A., and Shah, N.M. (2013). Sexually dimorphic neurons in the ventromedial hypothalamus govern mating in both sexes and aggression in males. Cell *153*, 896–909.

Yang, S.R., Hu, Z.Z., Luo, Y.J., Zhao, Y.N., Sun, H.X., Yin, D., Wang, C.Y., Yan, Y.D., Wang, D.R., Yuan, X.S., et al. (2018). The rostromedial tegmental nucleus is essential for non-rapid eye movement sleep. PLoS Biol. *16*, e2002909.

Ye, L., Allen, W.E., Thompson, K.R., Tian, Q., Hsueh, B., Ramakrishnan, C., Wang, A.C., Jennings, J.H., Adhikari, A., Halpern, C.H., et al. (2016). Wiring and Molecular Features of Prefrontal Ensembles Representing Distinct Experiences. Cell *165*, 1776–1788.

Yu, X., Li, W., Ma, Y., Tossell, K., Harris, J.J., Harding, E.C., Ba, W., Miracca, G., Wang, D., Li, L., et al. (2019). GABA and glutamate neurons in the VTA regulate sleep and wakefulness. Nat. Neurosci. *22*, 106–119.

Yuan, X.S., Wang, L., Dong, H., Qu, W.M., Yang, S.R., Cherasse, Y., Lazarus, M., Schiffmann, S.N., d'Exaerde, A.K., Li, R.X., and Huang, Z.L. (2017). Striatal adenosine $A_{2A}$ receptor neurons control active-period sleep via parvalbumin neurons in external globus pallidus. eLife *6*, e29055.

Yuzgec, O., Prsa, M., Zimmermann, R., and Huber, D. (2018). Pupil Size Coupling to Cortical States Protects the Stability of Deep Sleep via Parasympathetic Modulation. Curr. Biol. *28*, 392–400.e3.

Zhang, Z., Ferretti, V., Güntan, İ., Moro, A., Steinberg, E.A., Ye, Z., Zecharia, A.Y., Yu, X., Vyssotski, A.L., Brickley, S.G., et al. (2015). Neuronal ensembles sufficient for recovery sleep and the sedative actions of $\alpha$2 adrenergic agonists. Nat. Neurosci. *18*, 553–561.

Zhang, S., Xu, M., Chang, W.C., Ma, C., Hoang Do, J.P., Jeong, D., Lei, T., Fan, J.L., and Dan, Y. (2016). Organization of long-range inputs and outputs of frontal cortex for top-down control. Nat. Neurosci. *19*, 1733–1742.

## STAR★METHODS

### KEY RESOURCES TABLE

| REAGENT or RESOURCE | SOURCE | IDENTIFIER |
|---|---|---|
| Antibodies | | |
| anti-GFP for immunohistochemistry | Aves Labs | GFP-1020; RRID: AB_10000240 |
| anti-Fos | Santa Cruz | sc-52; RRID:AB_2106783 |
| anti-GFP for immunoprecipitation | Memorial-Sloan Kettering Monoclonal Antibody Facility | Htz-GFP-19F7 and Htz-GFP-19C8; RRID: AB_2716736 and AB_2716737 |
| Bacterial and Virus Strains | | |
| AAV2-EF1α-DIO-ChR2-eYFP | UNC Chapel Hill Vector Core | NA |
| AAVDJ-EF1α-DIO-ChR2-eYFP | Stanford University Virus Core | NA |
| AAV2-EF1α-DIO-iC++-eYFP | UNC Chapel Hill Vector Core | NA |
| AAV2-EF1α-DIO-eYFP | UNC Chapel Hill Vector Core | NA |
| AAV2-EF1α-DIO-hM3D(Gq)-mCherry | UNC Chapel Hill Vector Core | NA |
| AAV2-EF1α-DIO-hM4D(Gi)-mCherry | UNC Chapel Hill Vector Core | NA |
| AAV2-EF1α-DIO-mCherry | UNC Chapel Hill Vector Core | NA |
| AAV2-EF1α-DIO-taCasp3-TEVp | UNC Chapel Hill Vector Core | NA |
| AAV2-CAG-FLEx-TC$^{66T}$ | Addgene | 48331 |
| AAV2-CAG-FLEx-RG | Addgene | 74292 |
| rAAV2-retro-EF1α-DIO-mCherry | This paper | Tervo et al., 2016 |
| rAAV2-retro-EF1α-DIO-eGFP | This paper | Tervo et al., 2016 |
| RG-deleted, eGFP-expressing rabies virus | Gene Transfer Targeting and Therapeutics Core of Salk Institute | NA |
| Chemicals, Peptides, and Recombinant Proteins | | |
| Clozapine-N-oxide | Sigma-aldrich | C0832 |
| Critical Commercial Assays | | |
| SuperScript III kit | Invitrogen | 18080-051 |
| Accuprime Taq polymerase | Invitrogen | 12339-024 |
| AmpliTaq Gold 360 Master Mix | Invitrogen | 4398886 |
| Absolutely RNA Nanoprep kit | Agilent | 400753 |
| RNAscope Manual Fluorescent Multiplex kit V2 | Advanced Cell Diagnostics | 323100 |
| Deposited Data | | |
| TRAP RNA-Seq raw and analyzed data | This paper | GEO: GSE124681 |
| Experimental Models: Organisms/Strains | | |
| Mouse, *B6.129(Cg)-Fos$^{tm1.1(cre/ERT2)Luo/J}$* | The Jackson Laboratory | 021882 |
| Mouse, *B6;129S4-Gt(ROSA)26Sor$^{tm9(EGFP/Rpl10a)Amc/J}$* | The Jackson Laboratory | 024750 |
| Mouse, *Chat$^{Cre}$* | The Jackson Laboratory | 006410 |
| Mouse, *Slc17a6$^{Cre}$* | The Jackson Laboratory | 016963 |
| Mouse, *Cck$^{Cre}$* | The Jackson Laboratory | 012706 |
| Mouse, *Gal$^{Cre}$* | GENSAT | KI87; RRID: MMRRC_031060-UCD |
| Mouse, *Calca$^{Cre}$* | Dr. Richard D. Palmiter | NA |

(*Continued on next page*)

*Continued*

| REAGENT or RESOURCE | SOURCE | IDENTIFIER |
|---|---|---|
| Oligonucleotides | | |
| *Gad1* (sense/anti-sense): | This paper | NA |
| multiplex, CACAGGTCACCCTCGATTTT/TCTATGCCGCTGAGTTTGTG; | This paper | NA |
| nested, TAGCTGGTGAATGGCTGACA/CTTGTAACGAGCAGCCATGA | This paper | NA |
| *Slc17a6* (sense/anti-sense): | This paper | NA |
| multiplex, GCCGCTACATCATAGCCATC/GCTCTCTCCAATGCTCTCCTC; | This paper | NA |
| nested, ACATGGTCAACAACAGCACTATC/ATAAGACACCAGAAGCCAGAACA | This paper | NA |
| *Calca* (sense/anti-sense): | This paper | NA |
| multiplex, CCTGAAGTTCTCCCCTTTCCT / GAGGTCTTGTGTGTACGTGC; | This paper | NA |
| nested, ATGCAGATGAAAGCCAGGGA / TACTCAGATTCCCACACCGC | This paper | NA |
| *Cck* (sense/anti-sense): | This paper | NA |
| multiplex, TGTCTGTGCGTGGTGATGGC/ GCATAGCAACATTAGGTCTGGGAG; | This paper | NA |
| nested, ATACATCCAGCAGGTCCGCAA/ CAGACATTAGAGGCGAGGGGT | This paper | NA |
| *Chat* (sense/anti-sense): multiplex, ATGGCCATTGACAACCATCTTCTG/CCTT GAACTGCAGAGGTCTCTCAT; nested, same as multiplex. | This paper | NA |
| *Gal* (sense/anti-sense): | This paper | NA |
| multiplex, AGCCTTGATCCTGCACTGAC/ TGCACAGTGGACATGGTCTC; | This paper | NA |
| nested, AACCACAGATCATTTAGCGACAA/ CCCGGCCTCTTTAAGGTGC | This paper | NA |
| *eGFP In situ* hybridization probe | Advanced Cell Diagnostics | 400281 |
| *Slc17a6 In situ* hybridization probe | Advanced Cell Diagnostics | 319171 |
| *Chat In situ* hybridization probe | Advanced Cell Diagnostics | 408731 |
| *Slc32a1 In situ* hybridization probe | Advanced Cell Diagnostics | 319191 |
| *Calca In situ* hybridization probe | Advanced Cell Diagnostics | 417961 |
| *Calcb In situ* hybridization probe | Advanced Cell Diagnostics | 425511 |
| *Gal In situ* hybridization probe | Advanced Cell Diagnostics | 400961 |
| *Cck In situ* hybridization probe | Advanced Cell Diagnostics | 402271 |
| Software and Algorithms | | |
| MATLAB | MathWorks | R2014b |
| OpenEx software | TDT | N/A |
| ImageJ | NIH | https://imagej.nih.gov/ij/ |
| RNA-Seq by Expectation-Maximization | This paper | Li and Dewey, 2011 |

## CONTACT FOR REAGENT AND RESOURCE SHARING

Further information and requests for resources and reagents should be directed to and will be fulfilled by the Lead Contact, Yang Dan (ydan@berkeley.edu).

## EXPERIMENTAL MODEL AND SUBJECT DETAILS

*Fos*$^{CreER}$, *Gt(ROSA)26Sor*$^{EGFP/Rpl10a}$, *Chat*$^{Cre}$, *Slc17a6*$^{Cre}$ and *Cck*$^{Cre}$ (Jackson stock no: 021882, 024750, 006410, 016963, and 012706 respectively) were obtained from Jackson Laboratory. *Gal*$^{Cre}$ (stock no: 031060-UCD) was obtained from GENSAT. A new line of *Calca*$^{Cre:GFP}$ mice (version 2) was generated by replacing the Cre:GFP cassette in the original line (Carter et al., 2013) with a cassette containing an attenuated Cre recombinase; the nuclear localization signal was removed, the Kozak initiation codon was not optimal and the 3′ untranslated region was replaced with one from the *Myc* gene to destabilize the mRNA. These mice were using hybrid G4 ES cells (C57BL/6 × 129/Sv) and then backcrossed onto a C57BL/6 background for multiple generations. Mice were housed in 12 hr light-dark cycle (lights on at 07:00 am and off at 07:00 pm) with free access to food and water. Experiments were performed in adult male or female mice (2-6 months old). All procedures were approved by the Animal Care and Use Committees of the University of California, Berkeley.

## METHOD DETAILS

### Virus Preparation

AAV2-EF1α-DIO-ChR2-eYFP, AAV2-EF1α-DIO-iC++-eYFP, AAV2-EF1α-DIO-eYFP, AAV2-EF1α-DIO-hM3D(Gq)-mCherry, AAV2-EF1α-DIO-hM4D(Gi)-mCherry, AAV2-EF1α-DIO-mCherry, and AAV2-EF1α-DIO-taCasp3-TEVp were obtained from the University of North Carolina (UNC) vector core. AAV2-CAG-FLEx-TC$^{66T}$ (Addgene; plasmid #48331), AAV2-CAG-FLEx-RG (RG, rabies glycoprotein; Addgene; plasmid #74292), rAAV2-retro-EF1α-DIO-mCherry and rAAV2-retro-EF1α-DIO-eGFP (Tervo et al., 2016) were prepared in house according to previously described protocols (Hauswirth et al., 2000; Zhang et al., 2016). RG-deleted, eGFP-expressing rabies virus (RV*dG*) was purchased from Gene Transfer Targeting and Therapeutics Core of Salk Institute, amplified in B7GG cells, pseudotyped with BHK-EnvA cells, and titered with HEK293-TVA cells (Osakada and Callaway, 2013).

### Surgical Procedures

Adult mice (6-12 weeks old) were anesthetized with 1.5%–2% isoflurane and placed on a stereotaxic frame. Body temperature was kept stable throughout the procedure using a heating pad. After asepsis, the skin was incised to expose the skull, and the overlying connective tissue was removed. For EEG and EMG recordings, a reference screw was inserted into the skull on top of the left cerebellum. EEG recordings were made from two screws on top of the left and right cortex, at anteroposterior (AP) –3.5 mm, mediolateral (ML) 3 mm and AP +1.5 mm, ML 1.5 mm, respectively. Two EMG electrodes were inserted into the neck musculature. Insulated leads from the EEG and EMG electrodes were soldered to a pin header, which was secured to the skull using dental cement. Mice of specific genotype were randomly assigned to experimental and control groups. Experimental and control animals were subjected to exactly the same surgical and behavioral manipulations. Investigators were not blinded to animal identity and outcome assessment.

For optogenetic activation/inactivation experiments, a craniotomy (0.5-1mm diameter) was made on top of the target regions (see below for coordinates), and 0.1-0.3 μl virus was injected into the target regions using Nanoject II (Drummond Scientific) via a micro pipette. Optic fibers (0.2 mm diameter; Thorlabs) were implanted into the target region with the tip 0.2 mm above the virus injection site two weeks after viral injection. Dental cement was applied to cover the exposed skull completely and to secure the implants for EEG and EMG recordings to the screws. Data from all *Calca*$^{Cre}$ and *Cck*$^{-Cre}$ mice were included. For optogenetic experiment in *Slc17a6*$^{Cre}$ mice, data from 3 mice were excluded, because the tips of the optic fibers were in the dorsal periaqueductal gray. For chemogenetic experiments, ~0.2 μl AAV2-EF1α-DIO-hM3D(Gq)-mCherry or AAV2-EF1α-DIO-hM4D(Gi)-mCherry was injected into the target region. After surgery, mice were allowed to recover for at least 2 weeks before experiments.

For optrode recording experiments, a custom-made optrode assembly was inserted into the pIII region. The optrode assembly was secured to the skull together with EEG and EMG electrodes using dental cement.

For rabies-mediated retrograde transsynaptic tracing, ~0.3 μl of mixed AAV2-CAG-FLEx-TC$^{66T}$ and AAV2-CAG-FLEx-RG was injected into the target region of the corresponding Cre mice. Three weeks later, RVdG pseudotyped with EnvA was injected into the same region, and mice were sacrificed 5-6 days later for histology.

Stereotaxic coordinates for virus injection and optic fiber implantation:

pIII region: anteroposterior (AP) −3.8 mm, mediolateral (ML) 0 mm, dorsoventral (DV) 3.5 mm
Posterior ventromedial medulla: AP −6.9 mm, ML 0 mm, DV 5.7 mm
POA: AP 0 mm, ML 0.7 mm, DV 5.2 mm (unilateral)
LH: AP −1.8 mm, ML 1.5 mm, DV 5.0 mm (unilateral)
LS: AP 0.3 mm, ML 0.5 mm, DV 2.5 mm (unilateral)
MV: AP −6.0 mm, ML 0.5 mm, DV −3.8 mm (unilateral)

### Polysomnographic Recordings

Behavioral experiments were carried out in home cages placed in sound-attenuating boxes between 9:00 am and 7:00 pm. EEG and EMG electrodes were connected to flexible recording cables via a mini-connector. Recordings started after 20-30 min of habituation. The signals were recorded with a TDT RZ5 amplifier (bandpass filter, 1-750 Hz; sampling rate, 1,500 Hz). Spectral analysis was carried out using fast Fourier transform (FFT), and brain states were classified into NREM, REM and wake states (wake: desynchronized EEG and high EMG activity, NREM: synchronized EEG with high-amplitude, low-frequency (0.5-4 Hz) activity and low EMG activity, REM: high power at theta frequencies (6-9 Hz) and low EMG activity). The classification was made using a custom-written graphical user interface (programmed in MATLAB, MathWorks).

### Sleep Deprivation and Sleep Rebound Experiment

Sleep deprivation started at the beginning of the light period (7 am). Mice were kept awake by introducing novel objects or tapping lightly on the cages. To reduce the possibility of stress, mice were never touched directly. After 5 or 6 hr of deprivation, sleep-deprived mice were allowed rebound sleep in their home cages.

## Optrode Recording

Custom-made optrodes consisted of an optic fiber (200 μm in diameter) glued together with 6 pairs of stereotrodes. Two FeNiCr wires (Stablohm 675, California Fine Wire) were twisted together and electroplated to an impedance of ~200 kΩ using a custom-built plating device. The optrode was attached to a driver to allow vertical movement of the optrode assembly. Wires to record cortical EEG and EMG from neck musculatures were also attached for simultaneous recordings. A TDT RZ5 amplifier was used for all the recordings, signals were filtered (0.3-8 kHz) and digitized at 25 kHz. At the end of the experiment, an electrolytic lesion was made by passing a current (100 μA, 10 s) through one or two electrodes to identify the end of the recording tract.

Spikes were sorted offline based on the waveform energy and the first three principal components of the spike waveform on each stereotrode channel. Single units were identified automatically using the software KlustaKwik (http://klustakwik.sourceforge.net). The quality of each unit was assessed by the presence of a refractory period and quantified using isolation distance and L-ratio. Units with an isolation distance < 20 and L-ratio > 0.1 were discarded.

To identify ChR2-tagged neurons, laser pulse trains (15 and 30 Hz with duration of 1 and 0.5 s, respectively) were delivered every 1 or 2 min. A unit was identified as ChR2 expressing if spikes were evoked by laser pulses with high reliability (> 0.7 for all units in our sample), short first-spike latency (< 3 ms for all units in our sample), low jitter (< 2 ms for all units in our sample), and the waveforms of the laser-evoked and spontaneous spikes were highly similar (correlation coefficient > 0.9). To calculate the average firing rate of each unit in each brain state, spikes during the laser pulse trains were excluded.

## Optogenetic Manipulation

Each optic fiber was attached through an FC/PC adaptor to a 473-nm blue laser diode (Shanghai laser), and light pulses were generated using the TDT system. For all optogenetic activation experiments, each trial consisted of a 20 Hz pulse train (10 ms per pulse) lasting for 120 s. For optogenetic inactivation (60 s), constant light was used. For most experiments, the laser power was 4-6 mW at fiber tip. In *Slc17a6*$^{Cre}$ mice, the effects of optogenetic activation were different between low (1 mW) and high (3-5 mW) laser power. In *Calca*$^{Cre}$ and *Cck*$^{Cre}$ mice we have also tested the effects of laser at 10 mW (Figures S4B and S5G). In each optogenetic manipulation experiment, inter-trial interval was chosen randomly from a uniform distribution between 10 and 14 min, regardless of which brain state the animal is in. Each experimental session lasted for 3 hr, and each animal was tested in 6-8 sessions.

## Chemogenetic Manipulation

Saline (0.9% NaCl) or CNO dissolved in saline was injected intraperitoneally (i.p.) into the corresponding Cre mice expressing hM3D(Gq) or hM4D(Gi) in the target region. CNO dose was 1 mg/kg body weight for activation (in Gq-expressing mice) and 5 mg/kg body weight for inactivation (in Gi-expressing mice). For the control experiment (in mCherry-expressing mice), CNO (5 mg/kg) or saline was administered. Each recording session started immediately after injection. In each test set, mice were administered with saline on the first day and CNO on the second day. Each mouse was subjected to 3-4 test sets, and the data were averaged across all sets. For local chemogenetic activation of CALCA neuron axons, a guide cannula was inserted into the POA or posterior ventromedial medulla. CNO (3 μM, 50 – 100 nL) was intracranially microinjected into the target region.

## Pupillometry

The pupil was monitored with an infrared video camera at 30 Hz sampling rate. Video files were loaded into MATLAB, and each frame was converted to a binary image. The pupil was fitted with an ellipse using a custom-written MATLAB program to measure its area. For each session, the pupil size was normalized by the mean value during the 2 s preceding the laser stimulation.

## Slice Recording

AAVDJ-EF1α-DIO-ChR2-eYFP (500 nl) was injected into the pIII of *Cck*$^{Cre}$ or *Calca*$^{Cre}$ mice, and recording was made 2-4 weeks after injection. Slice preparation was according to procedures described previously (Xu et al., 2015). Briefly, mouse was deeply anaesthetized with 5% isoflurane. After decapitation, the brain was dissected rapidly and placed in ice-cold oxygenated HEPES buffered artificial cerebrospinal fluid (ACSF; in mM: NaCl 92, KCl 2.5, $NaH_2PO_4$ 1.2, $NaHCO_3$ 30, HEPES 20, glucose 25, sodium ascorbate 5, thiourea 2, sodium pyruvate 3, $MgSO_4 \cdot 7H2O$ 10, $CaCl_2 \cdot 2H_2O$ 0.5 and NAC 12, at pH 7.4, adjusted with 10 M NaOH), and coronal sections of the pIII were made with a vibratome (Leica). Slices (300 μm thick) were recovered in oxygenated NMDG-HEPES solution (in mM: NMDG 93, KCl 2.5, $NaH_2PO_4$ 1.2, $NaHCO_3$ 30, HEPES 20, glucose 25, sodium ascorbate 5, thiourea 2, sodium pyruvate 3, $MgSO_4 \cdot 7H_2O$ 10, $CaCl_2 \cdot 2H_2O$ 0.5 and NAC 12, at pH 7.4, adjusted with HCl) at 32°C for 10 min and then maintained in an incubation chamber with oxygenated standard ACSF (in mM: NaCl 125, KCl 3, $CaCl_2$ 2, $MgSO_4$ 2, $NaH_2PO_4$ 1.25, sodium ascorbate 1.3, sodium pyruvate 0.6, $NaHCO_3$26, glucose 10 and NAC 10, at pH 7.4, adjusted by 10 M NaOH) at 25°C for 1-4 h before recording. All chemicals were from Sigma.

Whole-cell recordings were made at 30 °C in oxygenated solution (in mM: NaCl 125, KCl 4, $CaCl_2$ 2, $MgSO_4$ 1, $NaH_2PO_4$ 1.25, sodium ascorbate 1.3, sodium pyruvate 0.6, $NaHCO_3$ 26, and glucose 10). Excitatory postsynaptic potentials (EPSPs) were recorded using a potassium-based internal solution (in mM: potassium gluconate 135, KCl 5, HEPES 10, EGTA 0.3, MgATP 4, $Na_2GTP$ 0.3, and sodium phosphocreatine 10, at pH 7.3, 290-300 mOsm) in the presence of $GABA_A$ receptor antagonist bicuculline (20 μM). The resistance of the patch pipette was 3-5 MΩ. The cells were excluded if the series resistance exceeded 40 MΩ or varied by more than 20% during the recording period. To activate ChR2, we used a mercury arc lamp (Olympus) coupled to the epifluorescence light path and

bandpass filtered at 450-490 nm (Semrock), gated by an electromagnetic shutter (Uniblitz). A blue light pulse (5 ms) was delivered through a 40 × 0.8 numerical aperture water immersion lens (Olympus) at a power of 1-2 mW. Data were recorded with a Multiclamp 700B amplifier (Axon instruments) filtered at 2 kHz and digitized with a Digidata 1440A (Axon instruments) at 4 kHz. Recordings were analyzed using Clampfit (Axon instruments).

### Single-Cell RT-PCR

At the end of each recording, cytoplasm was aspirated into the patch pipette, expelled into a PCR tube as described previously (Lambolez et al., 1992). The single cell RT-PCR protocol was designed to detect the presence of mRNAs coding for *Gad1*, *Slc17a6*, *Chat*, *Calca*, *Cck* and *Gal*. First, reverse transcription and the first round of PCR amplification were performed with gene-specific multiplex primer using the SuperScript III One-Step RT-PCR kit (12574-018, Invitrogen) according to the manufacturer's protocol. Second, nested PCR was carried out using AmpliTaq Gold 360 PCR kit (4398886, Invitrogen) with nested primers for each gene. All multiplex primers were designed to target two different exons to differentiate mRNAs from genomic DNA. The final PCR products were sequenced and verified. Amplification products were visualized via electrophoresis using 2% agarose gel.

Primers (5′ > 3′) for single-cell RT-PCR:

***Gad1 (sense/anti-sense):***

multiplex, cacaggtcaccctcgatttt/tctatgccgctgagtttgtg;
nested, tagctggtgaatggctgaca/cttgtaacgagcagccatga
Final product 200 bp

***Slc17a6 (sense/anti-sense):***

multiplex, gccgctacatcatagccatc/gctctctccaatgctctcctc;
nested, acatggtcaacaacagcactatc/ataagacaccagaagccagaaca
Final product 506 bp

***Calca (sense/anti-sense):***

multiplex, CCTGAAGTTCTCCCCTTTCCT /GAGGTCTTGTGTGTACGTGC;
nested, ATGCAGATGAAAGCCAGGGA/TACTCAGATTCCCACACCGC
Final product 100bp

***Cck (sense/anti-sense):***

multiplex, TGTCTGTGCGTGGTGATGGC/ GCATAGCAACATTAGGTCTGGGAG;
nested, ATACATCCAGCAGGTCCGCAA/ CAGACATTAGAGGCGAGGGGT
Final product 237 bp

***Chat (sense/anti-sense):***

multiplex,
ATGGCCATTGACAACCATCTTCTG/CCTTGAACTGCAGAGGTCTCTCAT;
nested, same as multiplex.
Final product 324 bp

***Gal (sense/anti-sense):***

multiplex, AGCCTTGATCCTGCACTGAC/ TGCACAGTGGACATGGTCTC;
nested, AACCACAGATCATTTAGCGACAA/ CCCGGCCTCTTTAAGGTGC
Final product 286 bp

### Immunohistochemistry and Fluorescence *in situ* Hybridization (FISH)

Mice were deeply anaesthetized and transcardially perfused with 0.1M PBS followed by 4% paraformaldehyde (w/v) in PBS. For fixation, brains were kept overnight in 4% paraformaldehyde. For cryoprotection, brains were placed in 30% sucrose (w/v) in PBS solution for 36-48 hr. After embedding and freezing, brains were sectioned into 20 (for FISH and a subset of immunohistochemistry) or 50-μm (for other immunohistochemistry) coronal slices using a cryostat. For immunohistochemistry, brain slices were washed using PBS three times, permeabilized using PBST (0.3% Triton X-100 in PBS) for 30 min and then incubated with blocking solution (5% normal goat serum or normal donkey serum in PBST) for 1 hr followed by primary antibody incubation overnight at 4°C using anti-GFP (GFP-1020, Aves Labs, 1:500) and anti-cFos (sc-52, Santa Cruz biotech, 1:500) antibodies. The next day, slices were washed with PBS and incubated with appropriate secondary antibodies for 2 hr (1:1000, All from Invitrogen): A-11039, Alexa Fluor 488 goat anti-chicken IgG and A-11012, Alexa Fluor 594 goat anti-rabbit IgG. FISH was done using RNAscope Multiplex Fluorescent Assays V2 according to the manufacturer's instructions (Advanced Cell Diagnostics). Fluorescence images were taken using a fluorescence microscope (Keyence BZ-X710), a confocal microscope (LSM 710 AxioObserver Inverted 34-Channel Confocal, Zeiss) and Nanozoomer.

### Translating Ribosome Affinity Purification

TRAP experiment was performed as previously described (Heiman et al., 2014; Knight et al., 2012; Nectow et al., 2015). Briefly, mice were sacrificed and the pIII region was rapidly dissected on ice with a dissection buffer (1x HBSS, 2.5 mM HEPES [pH 7.4], 4 mM NaHCO3, 35 mM glucose, 100 μg/ml cycloheximide). Tissues from 7-8 mice were then pooled, homogenized in the homogenization buffer (20 mM HEPES [pH 7.4], 150 mM KCl, 10 mM MgCl2, 0.5 mM DTT, 80 U/ml RNasin, 40 U/ml Superasin, 100 μg/ml cycloheximide and protease). Homogenates were transferred to a microcentrifuge tube and clarified at 2,000xg for 10 min at 4°C. The supernatant was transferred to a new tube, and 1/9 sample volume of 10% NP40 and 1/9 sample volume of 1,2-diheptanoyl-sn-glycero-3-phosphocholine (DHPC, 300mM) were added to the supernatant. This solution was mixed and then clarified at 20,000xg for 10 min at 4°C. The resulting supernatant was transferred to a new tube. This supernatant served as the input. A small amount (50 μl) was taken and added to a new tube containing 100 μL of lysis buffer from Absolutely RNA Nanoprep kit (Agilent) for future input RNA purification. The rest of the supernatant were used for immunoprecipitation with eGFP antibodies (Memorial-Sloan Kettering Monoclonal Antibody Facility; clone names: Htz-GFP-19F7 and Htz-GFP-19C8, bioreactor supernatant purity).

Immunoprecipitation was performed with an anti-eGFP antibody loaded biotinylated Protein L magnetic Dynabeads. The samples and beads were incubated for 1h at 4°C. The beads were washed four times using 0.35M KCl wash buffer (20 mM HEPES [pH 7.4], 350 mM KCl, 10 mM MgCl2, 0.5 mM DTT, 1% NP40, 40 U/ml RNasin, and 100 μg/ml cycloheximide). After the final wash the RNA was eluted by addition of lysis buffer (100 μL) to the beads. Beads were removed with a magnet. Both the input and IP RNAs are purified with Absolutely RNA Nanoprep kit (Agilent) and analyzed with an Agilent 2100 Bioanalyzer. cDNAs were generated and amplified with SMART-Seq® v4 Ultra® Low Input RNA Kit. cDNA libraries for RNA-seq were prepared with Illumina Nextera Library Prep Kit and analyzed on an Illumina HiSeq 2500. RNA-Seq data were analyzed with RSEM (RNA-Seq by Expectation-Maximization)(Li and Dewey, 2011). Transcripts with TPM (Transcripts Per Kilobase Million) > 1 were used for analysis.

## QUANTIFICATION AND STATISTICAL ANALYSIS

Statistical analysis was performed using MATLAB and SigmaPlot. All statistical tests were two-sided. The 95% confidence intervals (CI) for brain state probabilities were calculated using a bootstrap procedure: For an experimental group of $n$ mice, with mouse $i$ comprising $m_i$ trials, we repeatedly resampled the data by randomly drawing for each mouse $m_i$ trials (random sampling with replacement). For each of the 10,000 iterations, we recalculated the mean probabilities for each brain state across the $n$ mice. The lower and upper confidence intervals were then extracted from the distribution of the resampled mean values. To test whether a given brain state is significantly modulated by laser stimulation, we calculated for each bootstrap iteration the difference between the mean probabilities during laser stimulation and the preceding period of identical duration. The "n" number for each experiment is provided in the text and figure legends.

## DATA AND SOFTWARE AVAILABILITY

### Data Resources

The accession number for the raw and analyzed data files for the TRAP sequencing analysis reported in this paper is NCBI Gene Expression Omnibus: GSE124681.

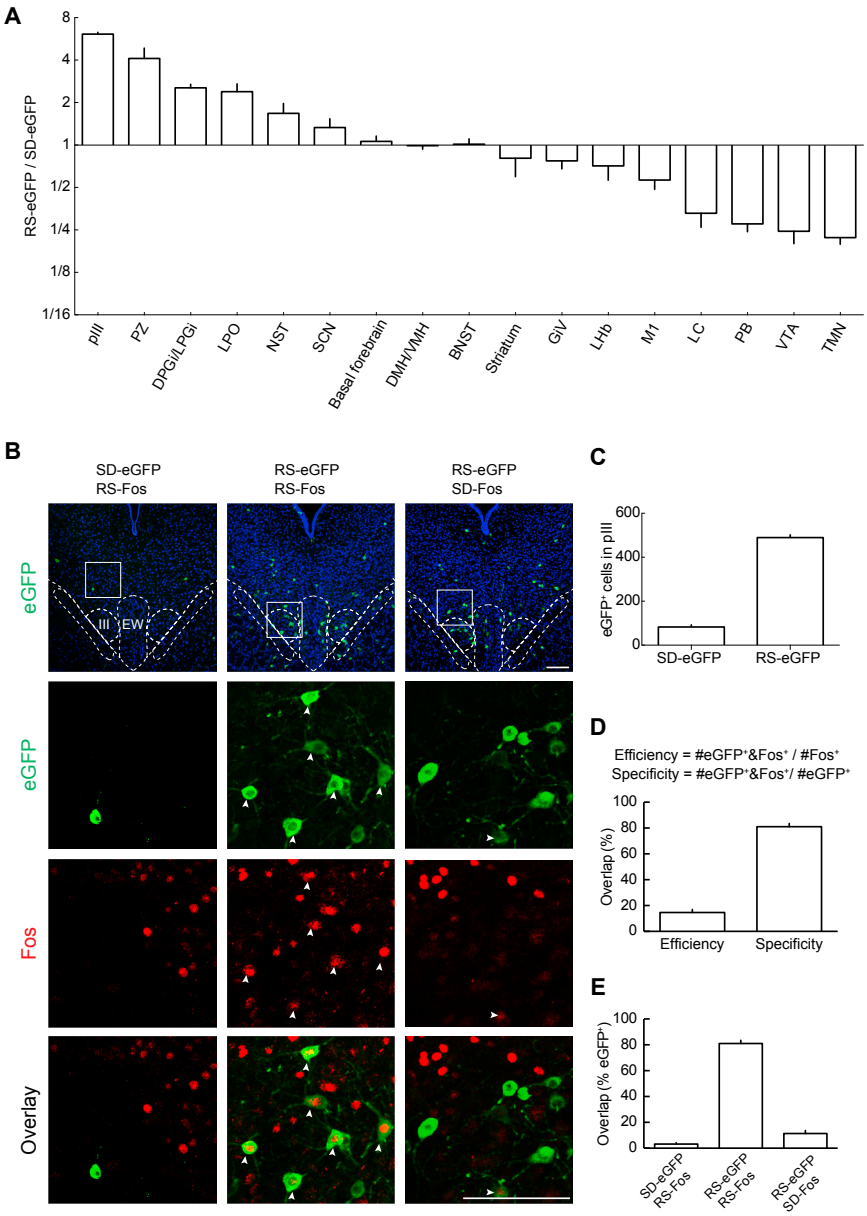


**Figure S1. Quantification and Control Experiments for Activity-Dependent Genetic Labeling, Related to Figure 1**

(A) Ratio between eGFP-labeled neurons in recovery sleep (RS) and sleep deprivation (SD) mice in multiple brain regions involved in sleep-wake regulation. Error bar, SEM; n = 5 pairs of littermates. pIII, perioculomotor region; PZ, parafacial zone; DPGi/LPGi, dorsal/lateral paragigantocellular nucleus; LPO, lateral preoptic area; NST, nucleus of the solitary tract; SCN, suprachiasmatic nucleus; DMH/VMH, dorsomedial/ventromedial hypothalamic nucleus; BNST, bed nucleus of the stria terminalis; GiV, gigantocellular reticular nucleus; LHb, lateral habenula; M1, primary motor cortex; LC, locus coeruleus; PB, parabrachial area; VTA, ventral tegmental area; TMN, tuberomammillary nucleus.

(B) Example images showing the overlap between eGFP and Fos expression in three groups of mice (at AP −3.7 mm). In each group, wake- or sleep-active neurons were first labeled with eGFP by pairing 4-OHT injection with SD or RS, respectively (Figure 1A). One week later, the mouse was sacrificed immediately following RS or SD for Fos immunohistochemistry. Scale bar, 100 μm. Blue, DAPI; green, eGFP; red, anti-Fos immunohistochemistry. Lower panels show enlarged views of regions in white boxes. Arrowheads indicate cells co-labeled with eGFP and Fos.

(C) Mean numbers of eGFP neurons in pIII of SD and RS mice. Error bar, SEM (n = 5 mice each).

(D) Efficiency and specificity of eGFP labeling in RS mice (mean ± SEM, n = 3 mice).

(E) Quantification of overlap between eGFP and Fos expression (mean ± SEM) in the three groups of mice shown in (B), n = 3 mice per group.

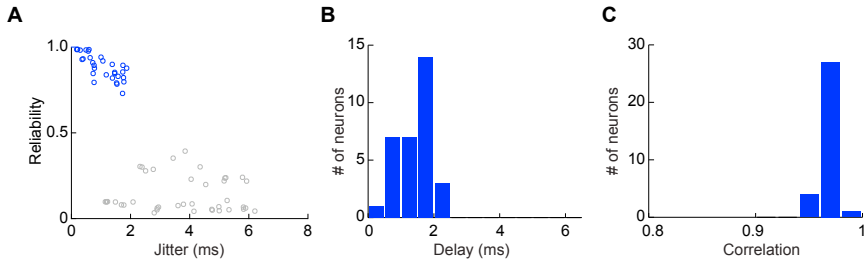


**Figure S2. Optogenetic Identification of CALCA Neurons in the pIII Region, Related to Figure 2**

(A) Reliability and temporal jitter of laser-evoked spikes in identified (blue) and unidentified (gray) units recorded in the pIII. Note that the identified and unidentified units form two distinct clusters, with high reliability and low jitter for identified units.

(B) Distribution of latencies of laser-evoked spiking for all identified CALCA neurons. Latency is defined as the timing of the first spike after each laser pulse.

(C) Distribution of Pearson correlation coefficients between laser-evoked and spontaneous spike waveforms for all identified units.

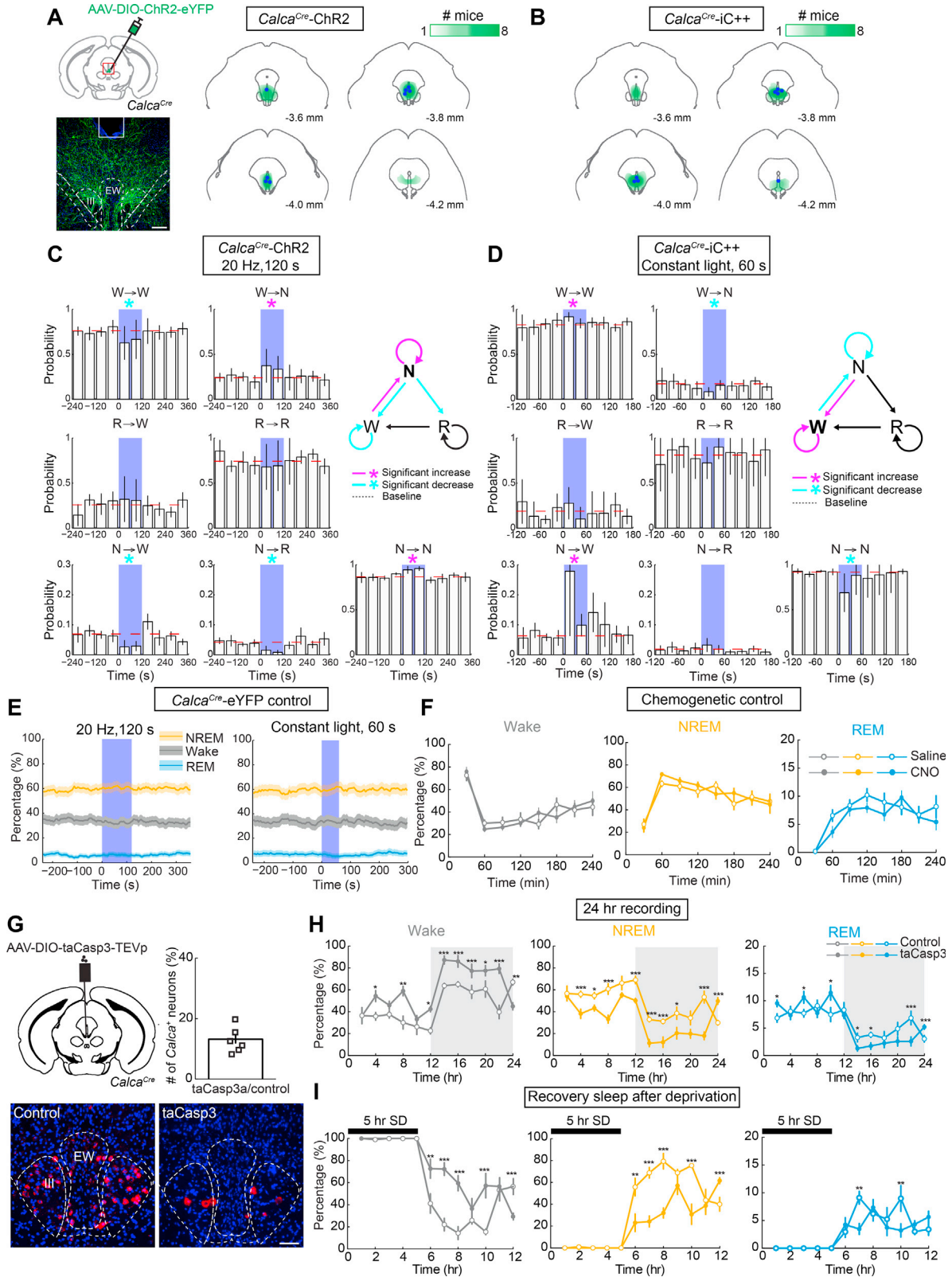


*(legend on next page)*

**Figure S3. Locations of pIII CALCA Neurons Targeted for Optogenetic Activation/Inactivation, Effects of Their Activation/Inactivation on Brain State Transition Probability, Control Optogenetic and Chemogenetic Experiments, and the Effect of Ablating pIII CALCA Neurons, Related to Figure 3**

(A) Left, fluorescence image of ChR2-eYFP expression in pIII (red box in coronal diagram, at AP −3.7 mm). Blue, DAPI; green, eYFP. Scale bar, 100 μm. Right, summary of ChR2-eYFP expression in *Calca*$^{Cre}$ mice. For each mouse (n = 8 mice), we determined the spread of ChR2-eYFP in 4 brain sections (from −3.6 mm to −4.2 mm along the rostrocaudal axis, where most of the virus expression was observed). The green color code indicates in how many mice the virus was expressed at the corresponding location. Blue dots indicate the locations of optic fiber tips.

(B) Similar to (A), for iC++-eYFP.

(C) Effect of optogenetic activation of CALCA neurons on transition probability between each pair of brain states. Each bar represents transition probability within each 20 s period (averaged across 3 consecutive 20 s bins within each 60 s). Error bar, 95% CI. Dashed line, baseline transition probability. N, NREM; R, REM; W, wake. Wake → REM and REM → N transitions are omitted because they were rarely detected with or without laser stimulation. Magenta/cyan asterisk (*) indicates significant increase/decrease in transition probability during laser stimulation compared to baseline ($p < 0.05$, bootstrap). The diagram summarizes transitions that are significantly increased (magenta) or decreased (cyan) by laser stimulation.

(D) Similar to (C), for optogenetic inactivation.

(E) Left, effect of 20 Hz laser stimulation in *Calca*$^{Cre}$-eYFP control mice. Shown is the percentage of time in NREM, REM, or wake state before, during, and after laser stimulation (120 s), averaged from 5 mice. Shading, 95% CI. Blue stripe, laser stimulation period. Right, for 60 s constant illumination (matching optogenetic inactivation protocol).

(F) Effect of CNO in *Calca*$^{Cre}$ mice expressing mCherry only. Shown is the percentage of time in each brain state following CNO or vehicle injection. Horizontal axis, time after CNO/vehicle injection. Error bar, ± SEM; n = 6 mice. There was no significant difference between CNO and vehicle injections ($p > 0.39$, 0.07, and 0.42 for NREM, REM and wake respectively for all data points; two-way ANOVA with Bonferroni correction).

(G) Ablation of pIII CALCA neurons. Left, schematic of virus injection into pIII. Middle, example images (at AP −3.8 mm) showing FISH of *Calca* (red) in pIII of mice injected with AAV-DIO-mCherry (control) or AAV-DIO-taCasp3-TEVp. Blue, DAPI. Scale bar, 100 μm. Right, ratio between the number of *Calca*-positive cells in mice injected with AAV-DIO-taCasp3-TEVp and that in their control litter mates injected with AAV-DIO-mCherry. Each symbol indicates one pair of litter mates.

(H) Effect of ablating CALCA neurons on sleep time. Shown is the percentage of time in each brain state over a 24 hr cycle in mice injected with control virus and AAV-DIO-taCasp3-TEVp. Error bar, ± SEM; n = 6 mice each. *$p < 0.05$; **$p < 0.01$; ***$p < 0.001$ (two-way ANOVA with Bonferroni correction).

(I) Similar to (H), during recovery sleep after 5 hr of sleep deprivation.

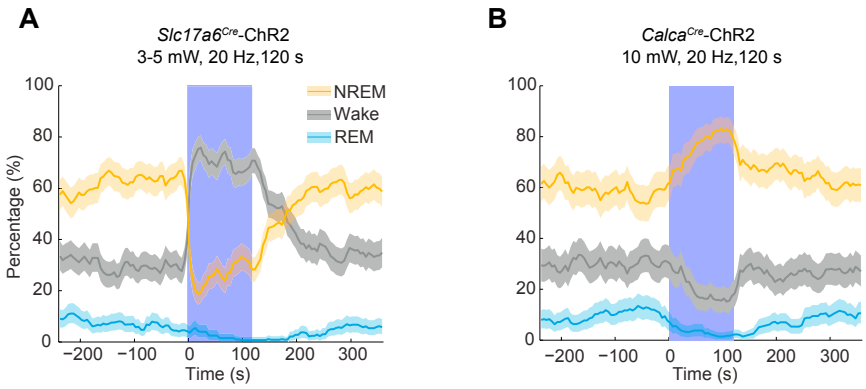


**Figure S4. Optogenetic Activation of pIII Neurons in *Slc17a6*$^{Cre}$ and *Calca*$^{Cre}$ Mice at High Laser Powers, Related to Figure 4**

(A) Laser stimulation at 3-5 mW in *Slc17a6*$^{Cre}$ mice. Shown is the percentage of time in NREM, REM, or wake state before, during, and after laser stimulation, averaged from 5 mice. Shading, 95% CI. Blue stripe, laser stimulation period (20 Hz, 120 s). Laser stimulation significantly decreased NREM sleep ($p < 0.0001$, bootstrap) and increased wakefulness ($p < 0.0001$).

(B) Laser stimulation at 10 mW in *Calca*$^{Cre}$ mice ($n = 4$ mice). Laser stimulation significantly increased NREM sleep ($p < 0.0001$, bootstrap) and decreased wakefulness ($p < 0.0001$) and REM sleep ($p < 0.0001$).

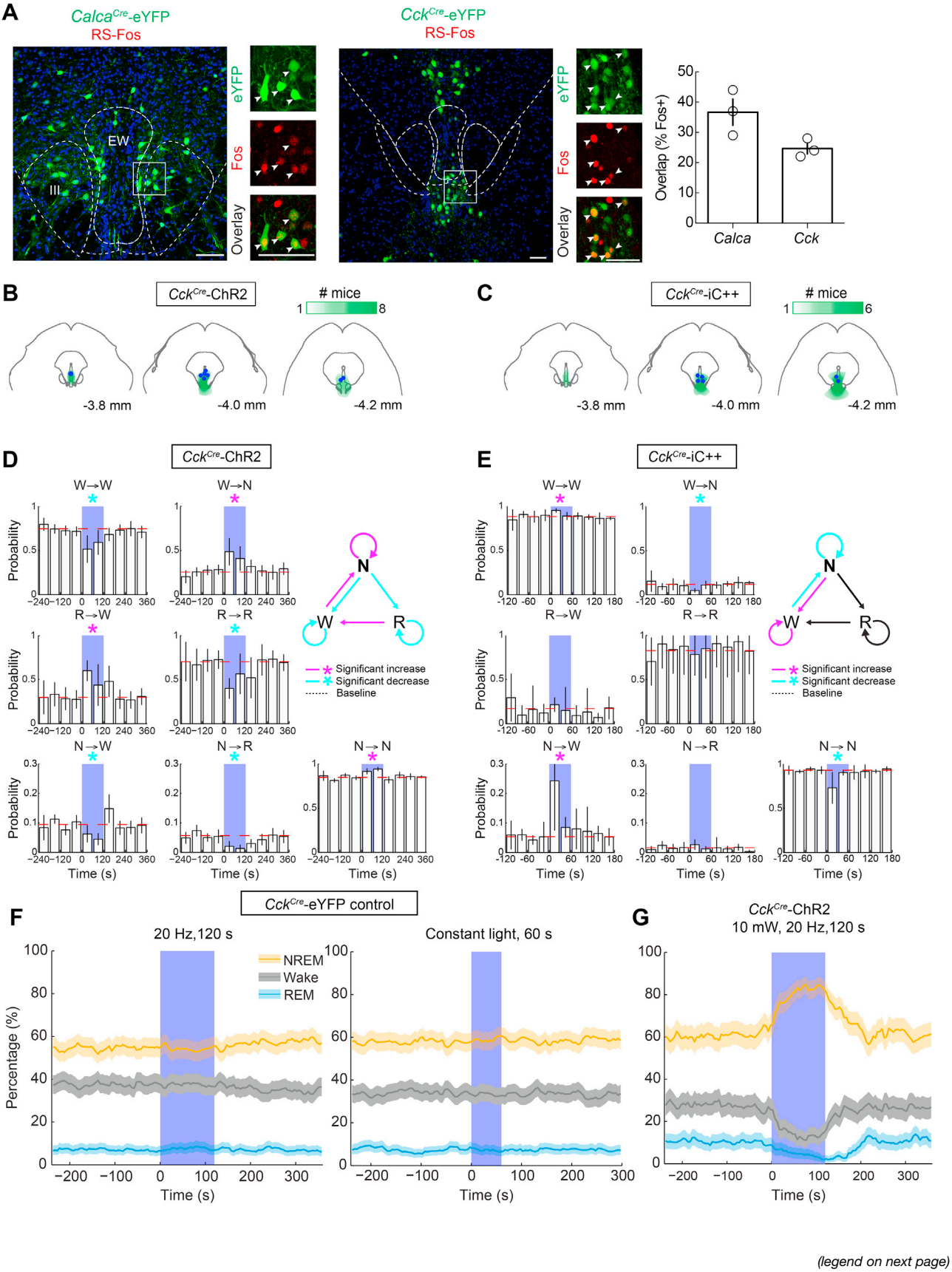


(legend on next page)

**Figure S5. Percentage of Sleep-Active Neurons that Are CCK and CALCA Neurons, Locations of pIII CCK Neurons Targeted for Optogenetic Activation and Inactivation, Effects of Their Activation and Inactivation on Brain State Transition Probability, Control for the Optogenetic Experiment, and the Effect of Activating CCK Neurons at High Laser Power, Related to Figure 5**

(A) Left/middle, example images showing the overlap between eGFP labeling of CALCA/CCK neurons and Fos expression in RS mice detected immunohistochemically (at AP −3.8 mm). Scale bar, 100 μm. Blue, DAPI; green, eGFP; red, anti-Fos immunohistochemistry. Arrowheads indicate cells co-labeled with eGFP and Fos. Right, percentage of Fos+ neurons that are CALCA or CCK neurons. Each symbol represents one brain sample. Bar, mean ± SEM.

(B) Summary of ChR2-eYFP expression in $Cck^{Cre}$ mice. For each mouse (n = 8 mice), we determined the spread of ChR2-eYFP in 3 brain sections (from −3.8 mm to −4.2 mm along the rostrocaudal axis, where most of the virus expression was observed). The green color code indicates in how many mice the virus was expressed at the corresponding location. Blue dots indicate the locations of optic fiber tips.

(C) Similar to (B), for iC++-eYFP.

(D) Effect of optogenetic activation of CCK neurons on transition probability between each pair of brain states. Each bar represents transition probability within each 20 s period (averaged across 3 consecutive 20 s bins within each 60 s). Error bar, 95% CI. Dashed line, baseline transition probability. N, NREM; R, REM; W, wake. Wake→REM and REM→N transitions are omitted because they were rarely detected with or without laser stimulation. Magenta/cyan asterisk (*) indicates significant increase/decrease in transition probability during laser stimulation compared to baseline ($p < 0.05$, bootstrap). The diagram summarizes transitions that are significantly increased (magenta) or decreased (cyan) by laser stimulation.

(E) Similar to (D), for optogenetic inactivation.

(F) Effect of laser stimulation (20 Hz and constant illumination) in $Cck^{Cre}$-eYFP control mice. Shown is the percentage of time in NREM, REM, or wake state before, during, and after laser stimulation (120 s or 60 s), averaged from 5 mice. Shading, 95% CI. Blue stripe, laser stimulation period.

(G) Effect of laser stimulation at 10 mW in $Cck^{Cre}$ mice (n = 4 mice). Laser stimulation significantly increased NREM sleep ($p < 0.0001$, bootstrap) and decreased wakefulness ($p < 0.0001$) and REM sleep ($p < 0.0001$).

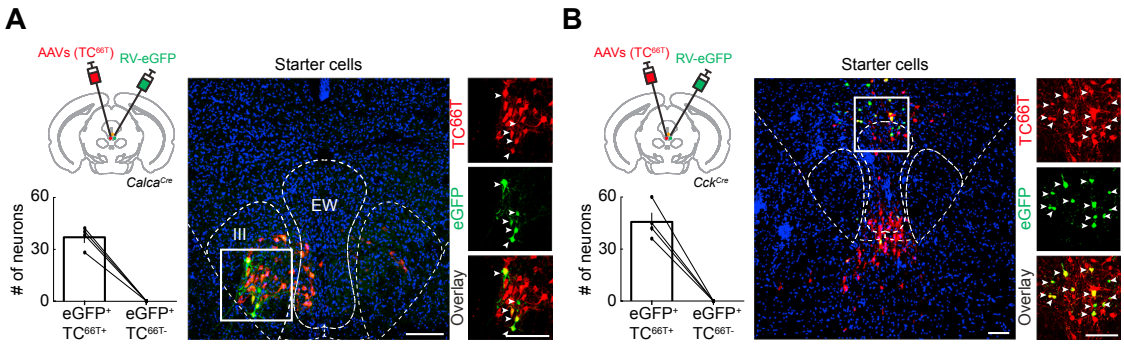


**Figure S6. Control for Rabies-Mediated Transsynaptic Tracing, Related to Figure 6**

(A) Control experiments for rabies-mediated transsynaptic retrograde tracing in *Calca*$^{Cre}$ mice. Left, schematic of virus injection. Middle, fluorescence image of pIII in a *Calca*$^{Cre}$ mouse (box in coronal diagram, at AP −3.8 mm). Right, region in white box showing starter cells (expressing both eGFP and mCherry, indicated by arrowheads); Blue, DAPI. Scale bar, 100 μm. Bar graph shows the numbers of starter cells and presynaptic neurons. Each line indicates data from one mouse (n = 4 mice).

(B) Similar to (A), for control experiment in *Cck*$^{Cre}$ mice (n = 4 mice). Shown is a coronal image at AP −3.8 mm.

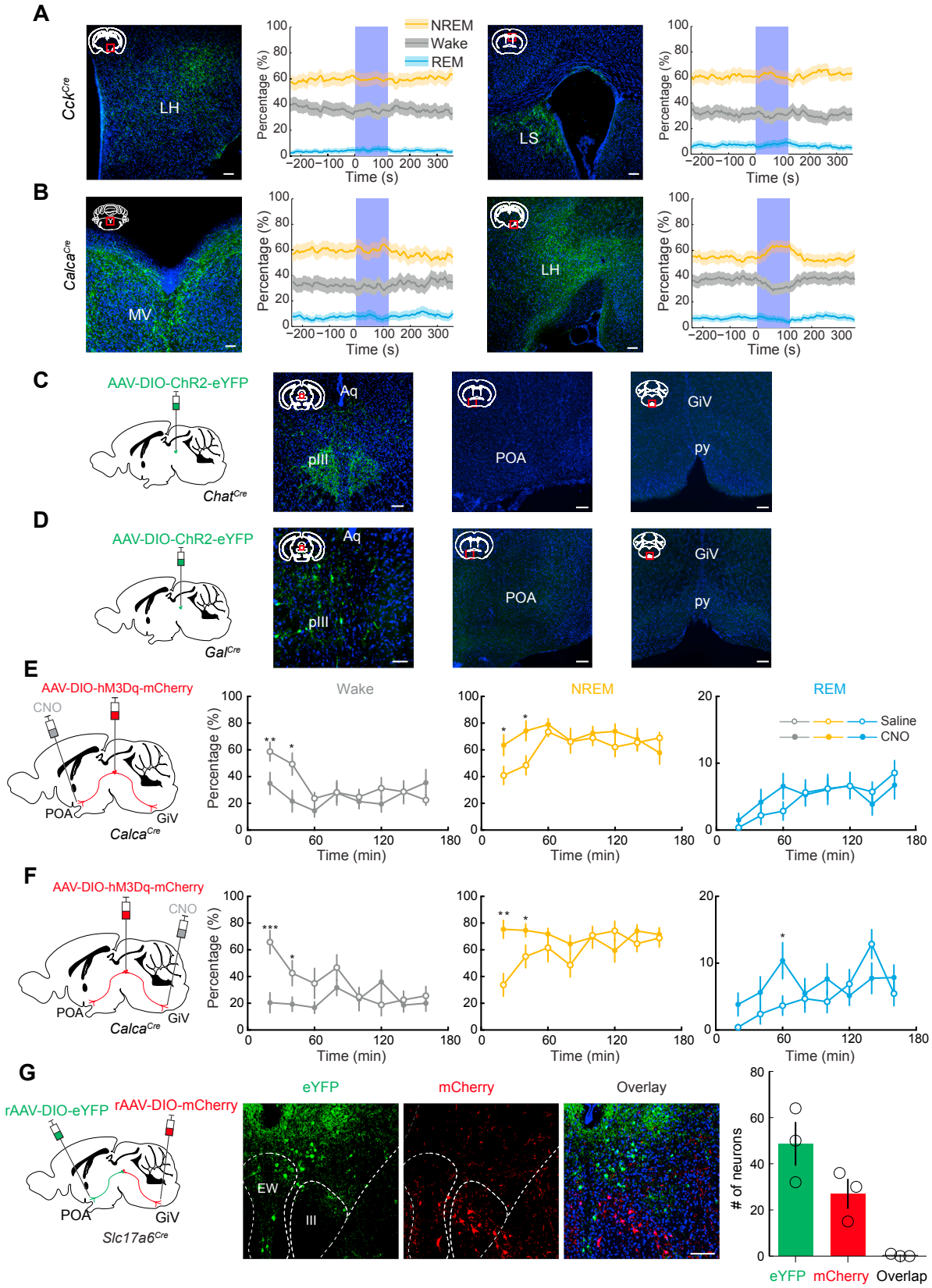


*(legend on next page)*

**Figure S7. Long-Range Projections of CCK and CALCA Neurons to Other Regions, Lack of Projection from Cholinergic and Galaninergic pIII Neurons to the POA and Posterior Medulla, Local Chemogenetic Activation of CALCA Neuron Axons in the POA and Medulla, and Dual Retrograde Tracing from the POA and Medulla, Related to Figure 7**

(A) Optogenetic activation of CCK neuron axons in the LH and LS had no effect. Left, fluorescence image of LH or LS (red box in coronal diagram) in a $Cck^{Cre}$ mouse injected with AAV-DIO-ChR2-eYFP into the pIII. Blue, DAPI. LH, lateral hypothalamus; LS, lateral septum. Scale bar, 100 μm. Right, percentage of time in NREM, REM, or wake state before, during, and after laser stimulation, averaged from 4 mice. Shading, 95% CI. Blue stripe, laser stimulation period (20 Hz, 120 s).

(B) Similar to (A), for optogenetic activation of CALCA neuron axons in the MV and LH. MV, medial vestibular nucleus. n = 4 mice.

(C) Fluorescence images of pIII, POA, and posterior ventromedial medulla (red box in coronal diagram) in a $Chat^{Cre}$ mouse injected with AAV-DIO-ChR2-eYFP in pIII, showing no projection to the POA or posterior ventromedial medulla. py, pyramidal tract. GiV, gigantocellular reticular nucleus.

(D) Similar to (C), for a $Gal^{Cre}$ mouse.

(E) Local chemogenetic activation of CALCA neuron axons in the POA. Shown is the percentage of time in each brain state following CNO or vehicle injection in $Calca^{Cre}$ mice expressing hM3D(Gq). Horizontal axis, time after CNO/vehicle injection. Error bar, ± SEM; n = 5 mice. *$p < 0.05$; **$p < 0.001$ (two-way ANOVA with Bonferroni correction).

(F) Similar to (E) for local chemogenetic activation of CALCA neuron axons in the posterior ventromedial medulla. n = 5 mice.

(G) Left, schematic for dual retrograde tracing of pIII glutamatergic projections to the POA and medulla. Middle, fluorescence image of the pIII showing eYFP and mCherry expression (at AP −3.8 mm). Right, number of neurons labeled by eYFP, mCherry, or both.